



VTOL AIRCRAFT

ME 492 PROJECT

Metin ÖZ

Harun ÜNER

Ömer KARATAŞ



Department of Mechanical Engineering
Boğaziçi University

Executive Summary

The technological innovations have been significantly shaping the aviation. These innovations mainly affected unmanned aircraft vehicles in the last decades. Among them, multi-copters have a dominant share. However, the flight time and payload have some disadvantages in these UAVs. That is why, the hybrid models like Vertical Take Off Landing aircrafts have been getting attention. These air vehicles are capable of horizontal and vertical flight. There are various configurations in terms of transition types and vertical flight types. This project intends to design a tiltrotor VTOL aircraft, because of its hover efficiency and compact structure.

In the design process, the purpose of project is explained. According to that, Product Design Specification is done. In this method, the important specifications like weight and control stability are listed. After that, the specifications are hierarchically organized. This is done by using Binary Dominance Matrix. In this method, specifications are listed with their importance weight. In the next step, possible design concepts are explained. These concepts have various rotor configurations and control mechanisms. The concepts are compared by the results of Binary Dominance Matrix. After the weighting, the concept of the project is selected.

The stated functional requirements give the wingspan, the take-off weight, and the cruise speed. According to that, airfoils are researched. The selection of airfoil is the most important part of the process, as they provide certain lift coefficient and drag coefficient for the selected Reynolds number. After that, the wing is designed by using XFLR5 software. This software is specifically used for small-scale fixed wing vehicles. With XFLR5, multiple iterations are done, until sufficient lift is acquired. After that step, tail is designed in XFLR5. The tail is responsible for the orientation of the aircraft by generating pitching and yawing movements. The other function of the tail is making the plane statically stable. Finally, a fuselage designed in the SolidWorks. In its design, physical integrity and the storage of electronics are the main considerations.

3D design of both wing and tail is carried out using SolidWorks. By using both Ansys and XFLR5, the bending moment and other factors are calculated for proper internal structure design. Simultaneously, dynamic stability analyses are carried out with XFLR5. Then, the motors and the battery and other electronics in the market research are selected accordingly.

3D printing is chosen for manufacturing the wing, the fuselage, and the tail because of its ease of use and flexibility. The parts are divided and properly redesigned to manufacture in 3D printing, due to size restrictions. Afterwards, the assembly is carried out with adhesive and supporting units. After the assembly of the individual parts is done, the VTOL is assembled. With that, the assembly of mechanical parts are accomplished. In the next process, electronic wiring is carried out.

In the next step, the autopilot is configured on the flight controller before the flight tests. The open source ArduPilot is preferred for the autopilot thanks to its large community support and detailed documentation. After the autopilot is configured, the flight tests are carried out in hover flight and horizontal flight including the transition stage.

As the planning of the project is not straightforward, some of the planning happened during the design process. However, it is mostly stuck to the initial planning, except minor changes. Project management shows the work distribution among the project members, as some of the work is done collectively. Finally, some of the problems faced in the design process are discussed.

Table of Contents

Executive Summary	1
1. Introduction	5
1.1. Fixed-winged Vertical Take-off Landing Air Vehicles	7
1.2. Project Objectives and Functional Requirements	11
2. Design Process	13
2.1. Design Criteria and Product Design Specifications	13
2.2. Overview of Possible Solutions	16
2.3. Detailed Design and Analysis	20
3. Manufacturing Process	32
3.1. Selection of Materials	32
3.2. Selection of Manufacturing Processes	33
3.3. Steps of Assembly Processes	35
3.4. Cost Analysis	42
4. Project Management	44
5. Discussion	47
6. Conclusion	49
References	51
Appendices	54

List of Figures

Figure 1.1 A Conventional Multi-Copter Drone. [3]	5
Figure 1.2 Comparison of Configuration Hover Efficiency. [4]	6
Figure 1.3 Euler Angles of the Air Vehicle with Body Orientation. [6]	6
Figure 1.4 F-35B Lightning Aircraft in Vertical Take-off Mode. [8]	7
Figure 1.5 A picture of V-22 Osprey. [9]	8
Figure 1.6 An Example of the Quad Plane Configuration. [10]	9
Figure 1.7 An Example of the Tail-Sitter Plane. [10]	9
Figure 1.8 An Example of Tiltrotor Drone. [10]	10
Figure 1.9 Pixhawk 6X Flight Controller from Holybro. [10]	10
Figure 1.10 Block Diagram of the Multicopter Control Algorithm from PX4. [11]	11
Figure 2.1 Product Design Specifications.	13
Figure 2.2 Wheel Chard of the Design Criteria.	15
Figure 2.3 An Example Configuration Diagram of the First Concept. [12]	16
Figure 2.4 An Example Configuration Diagram of the Second Concept. [13]	17
Figure 2.5 An Example Configuration Diagram of the Third Concept. [14]	18
Figure 2.6 Commonly Used Airfoils: (a) NACA-6412; (b) NACA-4412; (c) NACA-2412.	20
Figure 2.7 Polar Diagrams of Airfoils ($Re=100.000$).	21
Figure 2.8 Results of Force Analysis of the Final Wing Design.	22
Figure 2.9 Span-wise Free-Body Diagram of the Aircraft.	23
Figure 2.10 Constant Velocity (13.6 m/s) vs. AoA Analysis Results of the Aircraft with V-Tail.	24
Figure 2.11 The Numerical Deflection Analysis Results.	25
Figure 2.12 Longitudinal Modal Responses of the Vehicle.	26
Figure 2.13 Spiral Mode Modal Responses of the Vehicle.	27
Figure 2.14 Lateral Modal Responses of the Vehicle.	27
Figure 2.15 The Designation of Rotor Positions.	28
Figure 2.16 The Tilting Mechanism.	29
Figure 2.17 Wing Total Deformation Results of FEA for Horizontal Flight.	29
Figure 2.18 Wing Total Deformation Results of FEA for Vertical Flight.	30
Figure 2.19 Equivalent Stress on the Wing Results of FEA for Horizontal Flight.	30
Figure 2.20 Equivalent Stress on the Wing Results of FEA for Vertical Flight.	30
Figure 3.1 Ender3-S1 3D Printer.	33
Figure 3.2 Prusha Slicer User Interface.	33
Figure 3.3 Exploded View of the Tilt Mechanism.	35
Figure 3.4 Divided Parts of the Wing.	35
Figure 3.5 Tabs and Pin Holes Used on the Wing Sections.	36
Figure 3.6 Gluing the Wing and Applying the Activator.	36

Figure 3.7 The Fully Assembled Wing and Hinge.....	36
Figure 3.8 The CAD Model of Servo Cap used on the Wing.....	37
Figure 3.9 The Fully Assembled Fuselage.....	37
Figure 3.10 Front and Back Hatches on the Fuselage.....	37
Figure 3.11 Pin Holes of the Tail	38
Figure 3.12 The Fully Assembled V-Tail.....	38
Figure 3.13 Pixhawk 2.4.8 Flight Controller.	39
Figure 3.14 Mission Planer Full Parameter List Window.	40
Figure 3.15 Ardupilot Tricopter Standard Motor Enumeration. [22].....	41
Figure 3.16 Mission Planer Servo Output Window.....	42
Figure 4.1 The Progress Tree of VTOL Design Process.	44
Figure 4.2 The Gantt Chard of the Designing of the VTOL aircraft for ME429.....	45
Figure 4.3 The Gantt Chard of the Production of the VTOL aircraft for ME492.	46
Figure 5.1 An Example of XFLR5 User Interface.	47
Figure 5.2 The Element Quality Result of the Structural Analysis.....	48
Figure 5.3 The Jacobian Ratio Result of the Structural Analysis.....	48

List of Tables

Table 2.1 Binary Dominance Matrix.	15
Table 2.2 The Decision Matrix and Concept Evaluation.....	19
Table 2.3. Geometric Parameters and Analysis Results of Design Iterations.	21
Table 2.4 Geometric Properties of the V-Tail Stabiliser.	23
Table 2.5 The Geometric Properties and Multiplication Constants of Wing Section.....	24
Table 3.1 Mechanical Properties of PLA and ABS.....	32
Table 3.2 Manufacturing Time and Weight of the Printed Parts of the Vehicle.	34
Table 3.3 Usage areas and Properties of Copper Wires according to American Wire Gauge (AWG)....	40
Table 3.4 Changed VTOL Configuration Parameters and their definitions.	41
Table 3.5 The Overall Cost including every part.....	42
Table 3.6 The cost that is specifically allocated for the project	43

1. Introduction

In the aviation world, the technological innovations and new concepts have increased significantly in recent decades. Unmanned air vehicles are the focus of these developments. This can be largely attributed to their flexibility of use, new manufacturing techniques, the availability of electronic components and software. One of the main advantages of UAVs is their scalability. Conventionally, aircrafts have serious size limitation due to a need for pilot. Therefore, the manufacturing costs are quite expensive. On the other hand, UAVs have very large range of sizes. That allows creating significantly smaller air vehicles for various operations at a lower cost like the multi-copter in *Figure 1.1*. Additionally, new manufacturing techniques like 3-D printing and composite manufacturing allowed the sector to produce more complex parts without any serious cost for UAVs [1]. Furthermore, advancements in electronics and open-source software have accelerated the integration of complex control systems, sensors. These developments allowed the industry to create more sophisticated unmanned air vehicles with capabilities of precise navigation, real-time data transmission, and autonomous flight [2].



Figure 1.1 A Conventional Multi-Copter Drone. [3]

Among unmanned air vehicles, multi-copter drones are the most common type of UAVs, without a doubt. The decrease in the cost of electronics and the developments in control systems are the main drivers behind its popularity. Additionally, its ease of use and manoeuvrability makes it superior to other UAVs. Especially, this manoeuvrability becomes crucial in places where the space is limited, and there is a lack of runway. The use of multi-copter drones ranges from agriculture, military to entertainment. Despite its advantages, hover efficiency of this type of UAVs are significantly lower than fixed-wing UAVs [4]. As the graph in the *Figure 1.2* shows, its hover efficiency is significantly lower than the fixed-wing UAVs. Because of that, the flight time of drones are around 15-30 minutes, while fixed-wing UAVs can be up to multiple hours [2].

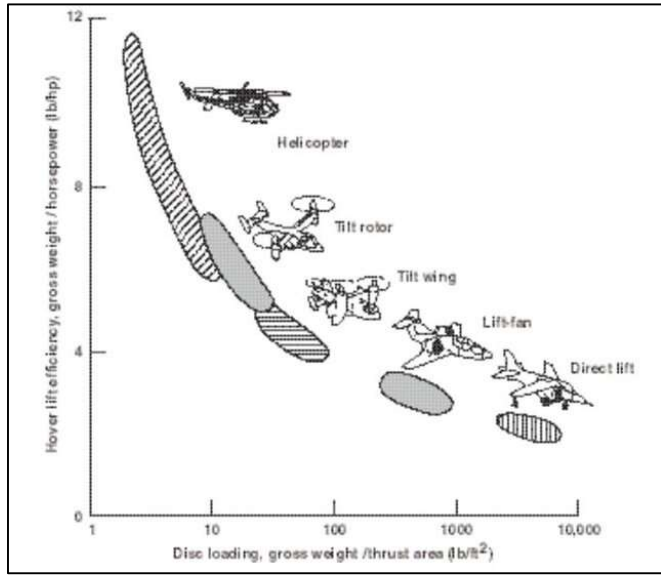


Figure 1.2 Comparison of Configuration Hover Efficiency. [4]

The take-off and landing of fixed-wing UAVs can be solved by using catapult systems or catching nets. The use of catapult systems is also used in military applications. However, accelerating air vehicles in a short period of time expose high stresses on the structure of UAVs. That limits the size and shape of UAVs and adds extra weight to endure high stresses. Furthermore, launching mechanisms adds additional transportation cost and may not be available in some applications. Therefore, the use of this system has its own limitation [5].

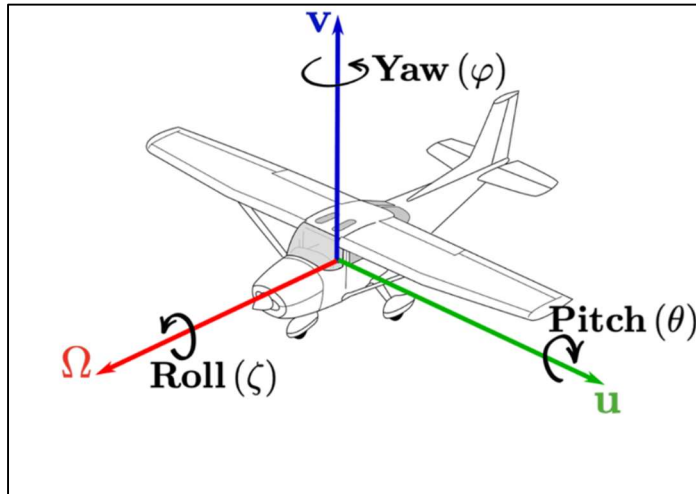


Figure 1.3 Euler Angles of the Air Vehicle with Body Orientation. [6]

For better understanding of the project, it is also important to understand key notations like Euler angles. The state of an aircraft is described by Euler angles. Euler angles, which are yaw, pitch and roll, refer to the angles made by the vehicle with the coordinate axes and the reference coordinate axes. These are shown in *Figure 1.3*. Yaw refers to the rotation of the aircraft around its vertical axis, which determines the direction the nose of the vehicle points horizontally. Pitch, on the other hand, describes the rotation around the lateral axis, controlling the upward or downward tilt of the nose. Finally, roll corresponds to the rotation around the longitudinal axis, which tilts the aircraft's wings. The movements that change these angles are called pitching, rolling and yawing, respectively. [6]

1.1. Fixed-winged Vertical Take-off Landing Air Vehicles

As stated in the previous parts, there is a significant trade-off between duration and a need for runway. While the hover efficiency of rotary wing aircraft can affect its flight time poorly, it also limits its range. Fixed winged conventional aircrafts can overcome this range issue with better hover efficiency and higher cruise speed, although it needs a serious infrastructure for take-off and landing. These concerns are the main motivations behind alternatives. That is why, vertical take-off landing air vehicles have caught great attention thanks to their hybrid nature. Vertical take-off landing air vehicles, VTOLs, has both forward flight and vertical landing and take-off capabilities. It can achieve this with several configurations. Technically, multi-copter drones are VTOLs, due to their both vertical and horizontal flight capabilities. Additionally, there are some UAVs with rotating wings which is also in the category of VTOLs. However, the term, VTOL, is generally used for fixed-winged VTOLs.

Fixed-wing VTOL aircrafts can perform high efficiency in their horizontal flight mode, like other conventional planes. They can also achieve vertical flight in limited spaces. Although every fixed-winged VTOLs have both forward and vertical flight capabilities, their configurations and how they managed the transition between vertical and horizontal flight can significantly differ.

Fixed-winged VTOLs are relatively new among other UAVs. But VTOLs are not only limited to UAVs. Fixed-winged VTOLs have been already in use in the US military. V-22 Osprey and F-35B are very successful example of VTOLs in military. The popularity of VTOLs mostly comes from their operational advantages in remote areas. Additionally, the popularity of V-22 Osprey comes from its superior flight range compared to rotorcrafts, as it is preferred over rotorcrafts for long range operations. Both V-22 Osprey and F-35B has marvellous engineering features and operates very differently.

F-35B Lightning II is a fifth-generation fighter jet equipped with a short take-off and vertical landing capabilities. Unlike other VTOLs, it operates its vertical flight by using his main jet engine with a use of fan system. Its rear nozzle design is one of the most engineering marvellous in aviation. It rotates the rear nozzle to redirect thrust for vertical flight. The hover flight mode configuration can be seen in *Figure 1.4*. In most cases, the vertical flight is not preferred during take-off and landing, because of high consumption of fuel. In war zones, the runway platforms can have serious damages, and the use of runway may not be possible. In these cases, most of fighter jets are not operable. This is the main hidden disadvantage of fighter jets. In these cases, the use of vertical take-off and landing have significant strategic importance. Compared to V-22 Osprey, its payload is significantly lower. The main difference between them is mechanism that used to produce thrust in vertical flight [7].

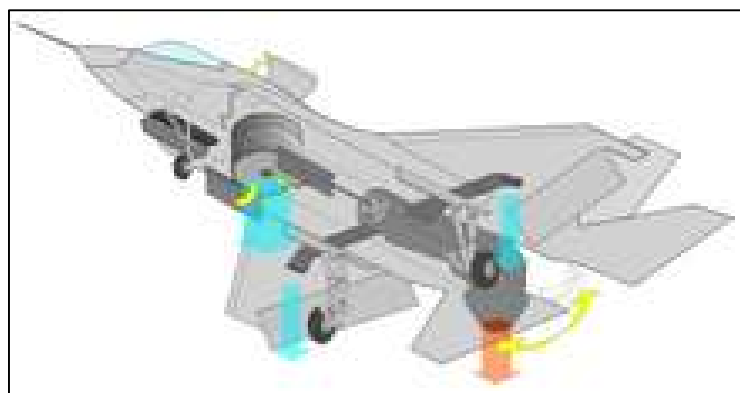


Figure 1.4 F-35B Lightning Aircraft in Vertical Take-off Mode. [8]

V-22 Osprey is an American multi-use, tiltrotor military cargo aircraft. Its purpose initially was to combine the features of helicopters with turboprop aircrafts. Its initiation started with the failure of Operation Eagle Claw by US military. In this operation, the conditions showed that there was clearly a need for air vehicle that can perform vertical landing and has high range in the military. During its development, the tilting mechanisms which rotates the orientation of thrust were quite new and required complex mechanical and control approaches. There were also additional factors like additional weight due to these mechanisms. These issues take multiple years to handle. V-22 Osprey has two Rolls-Royce AE 1107 engines connected at the edge of the wings with tilting mechanisms responsible for both vertical and horizontal flight. The engines are shown in the *Figure 1.5*. V-22 Osprey are commonly used for the logistical support for aircraft carriers for US army where the ranges are generally above the helicopter's range of operation and runway is insufficient for most cargo aircrafts [9].



Figure 1.5 A picture of V-22 Osprey. [9]

As F-35B and V-22 Osprey shown, VTOLs can achieve vertical and forward flight in various configurations. Mainly, fixed-winged VTOL UAVs are classified into three categories. These are Quad-in-Plane VTOL drones, tail-sitter VTOL drones, tiltrotor VTOL drones.

Quad-in-Plane drones have a very similar structure with normal fixed-wing UAVs. This type has two type rotors which separately dedicated to vertical thrust and horizontal propulsion as shown in *Figure 1.6*. During the take-off and landing, the vertical rotors in the plane are activated and produces necessary. Between the vertical and horizontal flight, the transition occurs, which the vertical rotors deactivated, and the horizontal rotors are activated. This type of drones offers easier control in tough conditions. During horizontal flight, the vehicle can be assisted by vertical thrust engines for agile turns or recovery manoeuvres. The multi-layer control algorithm allows that. Because of their stable control, they are often used in geospatial mapping and agriculture.

However, it has several disadvantages. Unused rotors in horizontal flight creates additional undesired drag. Since some of these rotors are located in wings. That can also lower the lift through turbulence. Considering these situations, it would not be wrong to assume that efficiency will decrease. However, due to the fact that the motor used as the horizontal propulsion motor differ from other motors, they show a more efficient horizontal flight performance than tiltrotor VTOLs. The reason for that is the fact that the motors have different kv values and can be combined with different propeller options to create combinations more optimised for horizontal flight. On the other hand, the unused rotors in the horizontal flight adds additional weight and slightly reduces the amount of payload that the vehicle can carry. [10]



Figure 1.6 An Example of the Quad Plane Configuration. [10]

Tail-sitter has relatively minimalist design. It achieves the transition through the rotation of the whole frame. It does not have any tilting mechanism or any specialized rotors. Initially the UAV is positioned vertically to achieve vertical flight as shown in *Figure 1.7*. After the take-off, the drone transitions to horizontal flight with the control of ailerons. This transition model removes the need for tilting mechanisms or any additional rotors for different functions. This simplicity makes it cost-effective and lightweight. However, the dynamic stability during transition phase requires more complex control algorithms, as the transition only occurs through the control of ailerons. In harsh weather conditions, this sophistication can make the flight impossible. Additionally, the vertical placement of the drone exposes high stresses on the frame. Making the drone structurally stable can consequently cause additional weight on the frame. These disadvantages limit the size of tail-sitter drones to small scale. These limitations limit the use of tail-sitter drones in tactical military operations and environmental monitoring. [10]



Figure 1.7 An Example of the Tail-Sitter Plane. [10]

Tiltrotor VTOL rotors have very similar to fixed-wing planes. It has two types of rotors. The vertical rotors are generally placed near the tail. The tilting rotors are placed in the wings. The tiltrotor drone in *Figure 1.8* shows this configuration. These tilting rotors have tilting mechanisms that enables the drone dual flight mode. In take-off and landing, the tilting mechanism rotates the rotors in vertical orientation. In transition, it gradually orients itself in horizontal position to achieve horizontal thrust. Compared to quad-in-plane drones, it can perform similarly without any additional weight and thrust. Moreover, it can have high payload unlike tail-sitter drones. These advantageous are the main motivation for the motivation behind choosing tiltrotor VTOL as the project.



Figure 1.8 An Example of Tiltrotor Drone. [10]

Another factor that plays an important role in the flight capability of the vehicles described above is the presence of a controller. The flight controller is an electronic system that controls actuators and maintains the stability of the vehicle. It could be the size of a computer in some large-scale vehicles, and the size of microcontrollers such as Arduino in small UAV drones. Their processing capabilities also vary according to their scale. The flight computers of large vehicles can simultaneously operate radars, cabinet systems, propulsion systems, fuel tanks, weapon rails and dozens of complex systems. On the other hand, drone flight controllers can only control simple tasks such as propulsion systems, control surfaces, vehicle positioning, ground station communication. Flight computers have multi-core processors operating at speeds of several GHz's, while flight controllers have 2-4 thread microcontrollers operating at speeds of several hundred MHz's.



Figure 1.9 Pixhawk 6X Flight Controller from Holybro. [10]

In *Figure 1.9* the Pixhawk-6X, the most advanced flight controller of the Holybro company, is shown. This flight controller with STM32-H753 microcontroller with up to 480MHz clock speed, 3 IMU sensors, 2 barometer sensors is a superior device in every sense. Thanks to UART, I2C CAN and even Ethernet connections, it can communicate and control many different peripherals.

As can be predicted, hardware without software is just an extra weight. Fortunately, there are 2 open-source software supported by flight controllers; Ardupilot and PX4. Although this two software, both written in C++, fulfil the same function, they have slight differences. PX4 can work with applications such as Simulink and Gazebo. With Simulink, the flight code can be bypassed and allow the developer to run his own flight code. In the Gazebo environment, this flight code can be simulated, and its performance can be evaluated. Ardupilot, on the other hand, targets the final user. The user can change many parameters without interfering with the flight code and can try developer updates. It has a clearer documentation and a larger community for support.

The flight code is the part of the code by which the propulsion and control surfaces are controlled to put the vehicle into the target state. It performs sensor fusion with the data it receives from IMU, barometer and GPS. For this, it uses instruments such as Kalman filter and Low Pass filter. States such as position, velocity, angle, angular velocity are calculated and fed into a cascading control algorithm to achieve the desired state. At each step, the independent PID algorithm is run and progresses in a stepwise manner from high level control to low level control. For example, the output of the position controller is converted into the input of the speed controller, the output of the speed controller is converted into the angle and so on. The final output is sent to the motor mixer to calculate the actuator states. A PWM signal is generated and transmitted to the actuators as an electrical signal. The control algorithm described is shown in the *Figure 1.10*.

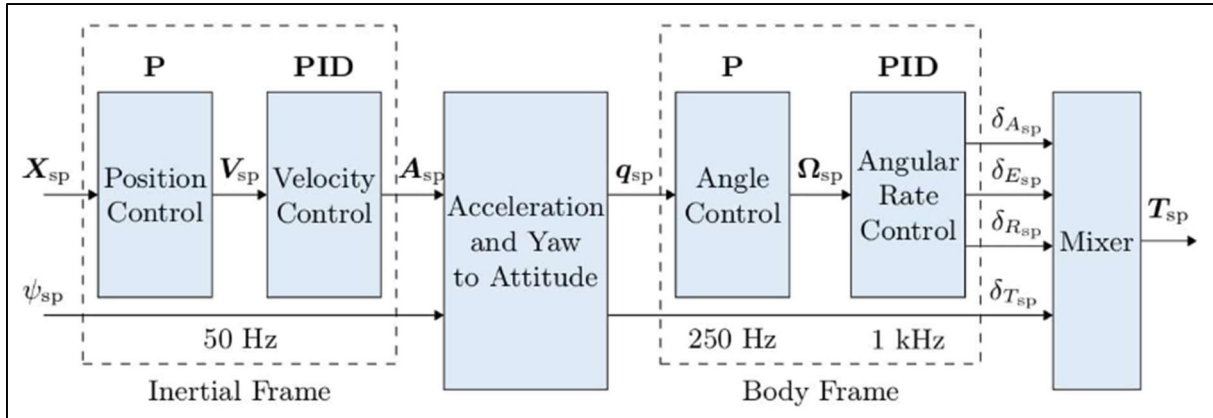


Figure 1.10 Block Diagram of the Multicopter Control Algorithm from PX4. [11]

1.2. Project Objectives and Functional Requirements

The main objective of this project is to design a functional fixed wing tiltrotor vertical take-off and landing (VTOL) aircraft. Today, fixed wing aircraft are outstanding for their efficiency and range in long distance flights. However, since they require long runways for take-off, their operational flexibility is limited. On the other hand, rotary wing aircraft, although they can be used in more compact areas thanks to their vertical take-off and landing capabilities, have disadvantages such as limited flight range and low speed. Combining the advantages of these two types of aircraft, the tiltrotor concept offers an innovative solution in the field of aviation.

Compared to other VTOLs, tiltrotor aircrafts perform better in both control stability and capability of payload. The use of same rotors horizontally and vertically with tilting mechanisms makes it more lightweight. The weight reduction should not be limited by the rotors themselves. Also, tilting mechanisms minimizes the additional structural elements that support each rotor. For

the small-scale applications, using multiple rotors for each flight mode as in Quad-in-Plane type may not be seen as big disadvantages, due to their light weight. However, as the scale increased like V-22 Osprey; the weight of the rotors can cause significant increase in the overall weight [6].

Within the scope of the project, a detailed design of the tiltrotor VTOL aircraft will be carried out. In this project, various simulations and calculations will be performed to analyse the aerodynamic performance, flight dynamics and structural strength of the aircraft. The dynamic model of the aircraft will be used to investigate the behaviour of the vehicle in various flight scenarios. 3D design activities will also be developed to optimise the FDM printed structure of the vehicle, and to achieve design objectives and functional requirements.

In the analysis phase of the project, the wing and tail design will be optimised to fly at low speeds. The forces and torques encountered in different flight modes (vertical take-off, cruise, vertical landing, etc.) will be evaluated in detail. Dynamic analyses will be performed to determine the flight stability of the vehicle, while structural strength analyses will be carried out to evaluate the strength of the tilt mechanism and wings under external loads. Since the vehicle parts will be produced by FDM 3D printing method, which is an anisotropic production method, material properties are important for structural analysis. For this reason, in-depth research on material properties will be required.

The scope the design is initially limited with specific requirements and limitations. The number of project members, limited time for the project, and the budget are the main considerations behind these requirements. The project is conducted by two members with a duration of one semester. Additionally, the budget for the project is only provided by the project members. These factors limited use of the electronics and the number of analyses to some extent. The specifications are decided with an extensive market research and the experiences of project members regarding the topic. In the research, similar aircrafts have been explored and this research has given certain idea about limitations and requirements for the projects. The Stallion-VTOL vehicle of the FLIGHTORY, which stands out with its similar features, was used to give an idea in the process.

The aircraft should follow the functional requirements given below.

Functional Requirements:

- Operating Conditions: VTOL is expected to operate in non-windy & clear weathers
- Semi-Autonomous Flight: The vehicle should be able follow a given flight path
- Tilt Rotor: The aircraft should have at least one tilt-rotor
- Manufacturing Constrain: Mostly 3D printable fuselage and wings
- Engine: Electrical power BLDC motors
- Power: 51.8-88.8Wh / 4s 16,8V 4500-6000mAh battery [$P_{Battery}$]
- Wing-Span: 1000-1500mm [L_{ws}]
- Take-off Weight: 1000-2000gr [M_{to}]
- Stall Speed: 8-10m/s [V_{Stall}]
- Cruise Speed: 10-13m/s [V_{Cruise}]
- Radio Control Range: Minimum of 300m
- Landing Gear: If it is essential for vertical take-off, 3-leg standoff

2. Design Process

2.1. Design Criteria and Product Design Specifications

In this part, design criteria are chosen according to the tiltrotor air vehicle. Product design specification is an extensive part that covers the essential prerequisites and necessary limitations and features. It is intended to lay out the important features in the tilt rotor air vehicles. For commercial products, Product Design Specification includes acceptance standards and disposal of the product regarding legislation and company policy. However, the project has no commercial interest. Therefore, acceptance standards and disposal regarding legislations are excluded from the selection of criteria. Product Design Specification which is shown in *Figure 2.1* can be classified in three categories as manufacturing requirements, performance requirements, and operation requirements.

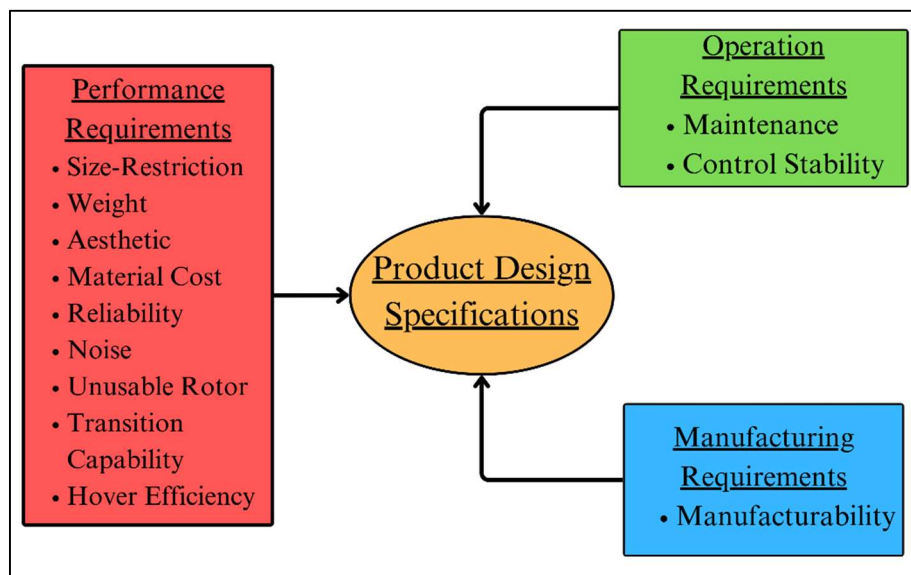


Figure 2.1 Product Design Specifications.

Performance Requirements:

Size-Restriction: In aviation, size can be very limiting factor for the motor and electronic options. Additionally, tiltrotor air vehicles have relatively complex structure due to their dual flight capabilities. That puts a minimum limit to its size due to the necessary electronics and battery. There is also restriction on upper limit due to the increasing complexity and other factors.

Weight: Although the weight of the aircraft can depend on the size of the aircraft, the weight is more multidimensional parameter. It depends on the lift of the air vehicle and largely on battery and frame. Unlike automotive industry, the weight is one of the most important parameters in aviation. For the projects, the requirements like battery and wingspan put additional importance on this criterion.

Aesthetic: Commercializing is not expected in the project. Consequently, the appeal of the consumer is out of concern. Despite that, the personal preferences in the project have given importance to this feature. Aesthetic can also be parallel with the functionality and practicality aspects of the product. These additional considerations made the aesthetic a part of the product design specification.

Cost: The project does not have a sponsorship or any fiscal incentive from any institution. The project is financed by the project members. Additionally, the cost of tiltrotor aircraft has wide range of variation, due to the electronics, especially the battery. These factors significantly limit the project as a whole.

Reliability: The aircraft is not intended to operate in risky operations. However, factors like the structural stability of the wings and the landing expose additional reliability issues for the operability. For the project, the aircraft should be operable at least multiple operations without being damaged.

Noise: The propellers are the main cause of noise in tiltrotor air vehicles. But factors like shape, size, and angular speed can significantly affect the intensity of the noise. The noise can have very limiting effect on the crowded area for noise pollution. That is why, noise is chosen as an important criterion.

Unusable Rotor: The efficient use of rotors has importance both on payload increase and the drag of the aircraft. In horizontal flight, the tiltrotor aircraft disables the vertical rotors for only horizontal thrust. This causes unusable rotors during that phase. Especially the placement of the vertical rotors around the airflow of wings can create significant turbulence which affects the aerodynamic efficiency poorly. In that sense, the unusable rotor is very crucial specification.

Transition Capability: The main feature of VTOL air vehicles is their capabilities in both hover and horizontal flight. This occurs through transition. Transition can affect the performance of the plane in terms of power consumption, stability. In some configurations, the transition can be very poorly in windy conditions and the transition may not even occur. These considerations have made a vital specification for the project.

Hover Efficiency: Similar to transition capability, hover efficiency is very crucial for the power consumption. Especially in tiltrotor VTOLs, during vertical flight mode, the motors consume a significant amount (about 25-40%) of battery energy.

Manufacturing Requirements:

Manufacturability: Manufacturability stands for the construction of frame including fuselage, tail, and wing. It also includes assembly process of the frame with electronics. The manufacturing capabilities are limited by the equipment in the laboratories of Bogazici university. Electronics is expected to be by external manufacturers. The general role of manufacturing and other factors gives manufacturability its importance in our project.

Operation Requirements:

Maintenance: Maintenance is a critical factor in ensuring the long-term functionality and safety of the tiltrotor air vehicle. Regular maintenance is not necessary for the project because of its limited use. After the operation, the plane should have a structure are easy to be inspected for any fracture in the frame. Additionally, the placement of the plane should be suitable to inspection.

Control Stability: For tiltrotor air vehicles, control stability has a vital role. Hover flight requires accurate adjustments of the rotors in case of disturbances. Transition phase requires significant amount of stability. Also, air vehicles expose to various disturbances. For these conditions, control stability of the plane is crucial. Poor control stability can even cause to crash of the plane. All these considerations render control stability as a vital specification in the project.

Table 2.1 Binary Dominance Matrix.

Criteria	Maintenance	Size-Restriction	Weight	Control Stability	Aesthetic	Material Cost	Manufacturability	Reliability	Noise	Unusable-Rotor	Transition Capability	Hover Efficiency	Total	Weighting
	#	1	0	0	0	0	0	0	1	0	1	0	3	0.045
Maintenance	#	1	0	0	0	0	0	0	1	0	0	0	1	0.015
Size-Restriction	0	#	0	0	0	0	0	0	1	0	0	0	0	0.106
Weight	1	1	#	0	1	1	1	0	0	1	1	1	0	7
Control Stability	1	1	1	#	1	1	1	1	1	1	1	1	11	0.167
Aesthetic	1	1	0	0	#	1	0	0	1	1	1	1	0	6
Material Cost	1	1	0	0	0	#	0	0	1	1	1	1	0	0.076
Manufacturability	1	1	1	0	1	1	#	0	1	1	1	1	9	0.136
Reliability	1	1	1	0	1	1	1	#	1	1	1	1	10	0.152
Noise	0	0	0	0	0	0	0	0	#	0	0	0	0	0.000
Unusable-Rotor	1	1	0	0	0	0	0	0	1	#	1	0	4	0.061
Transition Capability	0	1	0	0	0	0	0	0	1	0	#	0	2	0.030
Hover Efficiency	1	1	1	0	1	1	0	0	1	1	1	#	8	0.121
Sum of Total:												66	1	

As Product Design Specification is done. These specifications must be hierarchically organized to enable successful selection in the concept models. These specifications are listed in Binary Dominance Matrix which can be seen in *Table 2.1*. The purpose of the binary dominance matrix is to organize the features according to their importance. The features are placed in both columns and rows. Then, the specifications are compared to each other. This gave a value for each specification. From that, the weight of the specifications is calculated. The weights of the criteria are shown as a wheel card in *Figure 2.2* for a visual expression. Since the weight of the noise aspect is 0, it is not shown in the figure. With that method, it is concluded that control stability and reliability are the most important features, while noise is the least important feature for the project. This stems from the major role of control stability and the relative negligibility of noise.

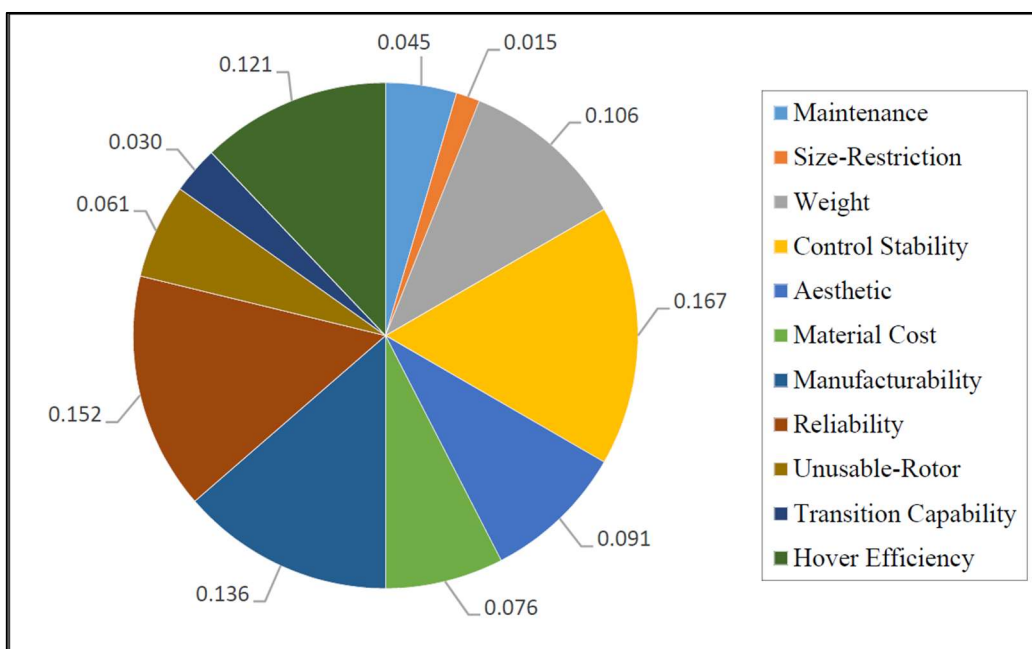


Figure 2.2 Wheel Chard of the Design Criteria.

2.2. Overview of Possible Solutions

When vertical take-off and landing aircraft are considered, it is observed that VTOL vehicles are differentiated from each other mainly by the number of rotors and the configurations of these rotors. Before starting the detailed design, the technical and practical benefits provided by different configurations were comprehensively evaluated in order to determine the most suitable configuration. The strengths and weaknesses of each alternative were taken into account to determine the configuration most compatible with the design objectives. During this evaluation process, each concept design was scored according to the criteria mentioned in Section 2.1 and the final concept design was determined using a decision matrix.

Concept 1: Three-Rotor VTOL

The first concept, the 3-rotor concept, is shown in *Figure 2.3*. In the three-rotor concept design, the front two rotors can rotate on the pitch axis, while the rear rotor generates thrust only during vertical take-off and landing. The front motors generate upward lift during vertical flight and change their tilt angles which are shown with α_1 in *Figure 2.3* to provide forward thrust when the flight mode is switched to horizontal flight. The rear motor is used to increase total lift and to stabilise the aircraft during vertical flight. It is disabled during horizontal flight. [12]

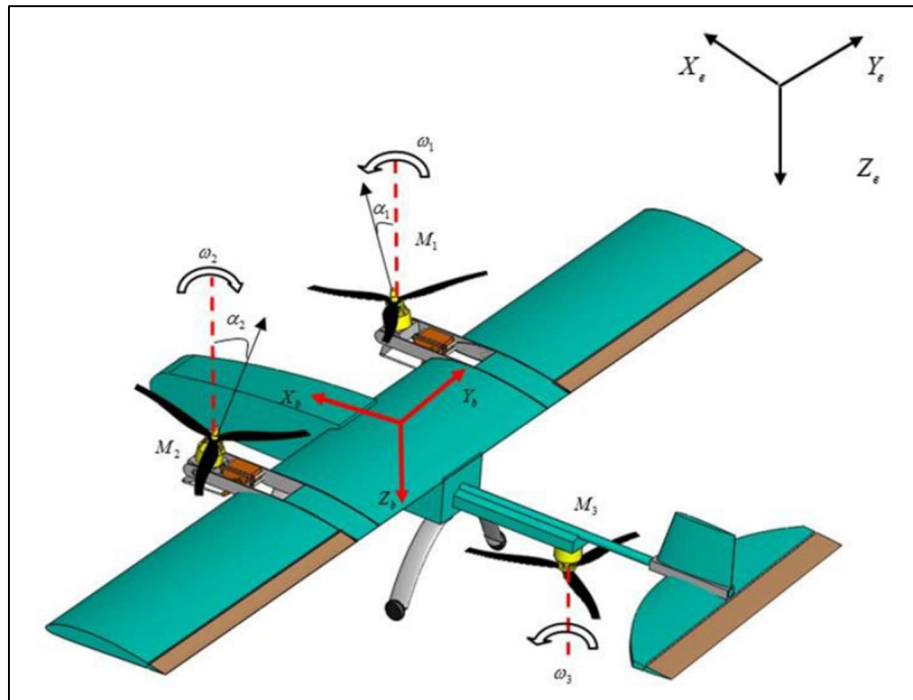


Figure 2.3 An Example Configuration Diagram of the First Concept. [12]

The movement of the aircraft in the longitudinal axis is achieved by generating a non-zero horizontal force by the front-positioned motors. The downward tilt of the two front motors results in a forward motion while speeding up rotors to keep the total vertical force constant.

The movement of the aircraft in the yaw axis is achieved by tilting the front motors in different directions. Meanwhile, the motors are speeding up in order to keep the vertical component of the thrust constant. While the coupled forces which are horizontal components of the thrust in different directions eliminate each other, it creates a nonzero moment in the yaw axis.

The movement of the aircraft in the roll axis is achieved by one of their front motors speeding up and the other slowing down. Thus, while the force remains constant on the vertical axis, a nonzero moment is generated on the roll axis.

During the transition, the front motors accelerate and tilt downwards. As the horizontal speed increases, generated lift by the wing increases, and the rear motor starts to slow down. When the vehicle reaches the cruise speed, the front motors are fully tilted and the rear motor is completely stopped. Hence, the horizontal flight mode begins. [10]

Concept 2: Four-Rotor VTOL

The second concept, the 4-rotor concept, is shown in *Figure 2.4*. In the four-rotor concept design, the front two rotors can rotate on the pitch axis, while the rear two rotors generate thrust only during vertical take-off and landing. The front motors generate upward lift during vertical flight and change their tilt angles which are shown with δ in *Figure 2.4* to provide forward thrust when the flight mode is switched to horizontal flight. The rear motors are used to increase total lift and to stabilise the aircraft during vertical flight. It is disabled during horizontal flight [13].

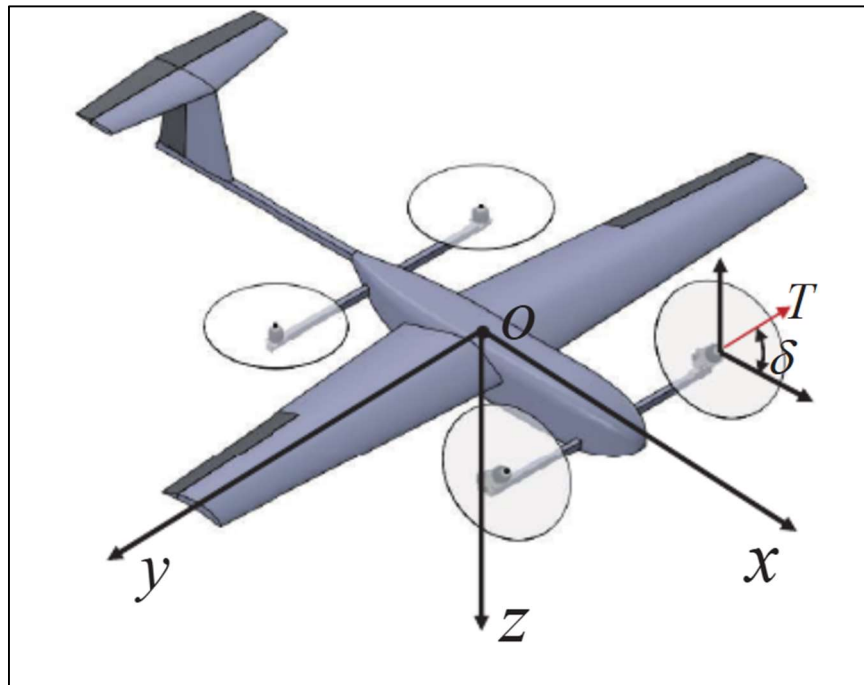


Figure 2.4 An Example Configuration Diagram of the Second Concept. [13]

The movement of the aircraft in the longitudinal axis is achieved by generating a non-zero horizontal force by the front-positioned motors. The downward tilt of the two front motors results a forward motion while speeding up rotors to keep the total vertical force constant.

The movement of the aircraft in the yaw axis is achieved by the rotation at different speeds of pairs of motors which are rotated in the same direction and positioned diagonally. The left-front and right-rear motor rotate in clockwise direction, while the right-front and left-rear motor rotate in counter-clockwise direction. These pairs rotating at different angular speeds produce a nonzero torque while keeping the vertical force constant.

The movement of the aircraft in the roll axis is achieved by motors at one side speeding up and the others slowing down. Thus, while the force remains constant on the vertical axis, a nonzero moment is generated on the roll axis.

During the transition, the motors at the front will accelerate and tilt downwards. As the horizontal speed increases, the amount of lift generated by the wing increases and the rear motors begin to slow down. The front motors are fully tilted and the rear motor is completely stopped when the vehicle reaches cruising speed. It is the start of the horizontal flight [10].

Concept 3: Two-Rotor VTOL

The last concept, the 2-rotor concept, is shown in *Figure 2.5*. In the two-rotor concept design, there are only two motors and is actively used in the both horizontal and vertical flight operation. The motors are positioned at the wing tips, and they can rotate in pitch axis. The challenging part of this design is to position the centre of gravity precisely on the line of intersection of the rotors. Otherwise, the couple forces create a moment in the pitch axis in vertical flight.

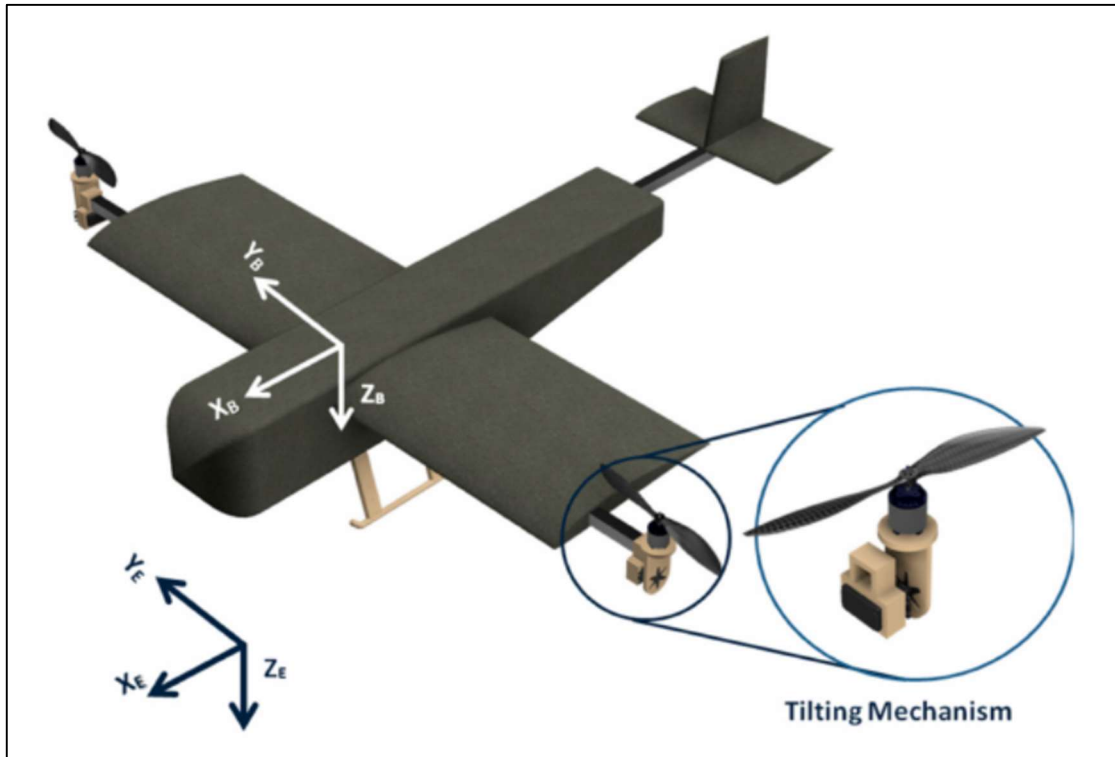


Figure 2.5 An Example Configuration Diagram of the Third Concept. [14]

The movement of the vehicle in the longitudinal axis is achieved by tilting the motors forwards, as in other concepts. The downward tilt of the both motors results a forward motion while speeding up rotors to keep the total vertical force constant.

The movement of the vehicle on the yaw axis is achieved by tilting the motors in different directions. The thrust produced by each motor will increase until the total of the vertical component of the thrusts balances the weight of the vehicle.

The roll movement of the vehicle is achieved by increasing the thrust produced by the rotor on one side and decreasing the other. During the roll movement, the total thrust in the vertical direction does not change. However, the sum of the torques generated by the rotation of the motors will become a non-zero value. In order to eliminate this torque, the motors are slightly tilted in the opposite directions to generate counter-yaw torque.

During transition, the motors are slowly tilted forwards. However, unlike other concept vehicles, there is no motor to generate pitching moment in the positive direction. Therefore, if the vehicle stalls during the transition, it is very difficult to recover it. Although this concept is more efficient than the others, it has serious negatives in both design and control.

Concept Evaluation

Decision matrix is a systematic decision-making tool used to select the most appropriate one among multiple options or alternatives. This method enables the scoring and comparison of alternatives according to the specified criteria. the option with the highest score in total is preferred. Decision matrix is frequently used in engineering designs or in situations where a large number of variables are evaluated to create an objective and fact-based decision mechanism.

The decision matrix shown in *Table 2.1* was used to evaluate the mentioned concepts. Each concept was evaluated by the group members for the stated criterion. Each group member ranked the concepts for their success in that criterion. The leading concept was given 3 points, the next one 2 points and the least one 1 point. Then the scores given by each group member were summed up. The summation constitutes the individual score of each concept for that criterion. The total score of the concept was calculated by summing the weighted scores of each concept from the criteria. The scores for criterion and total scores of the concepts are shown in *Table 2.2*.

Table 2.2 The Decision Matrix and Concept Evaluation.

Criteria	Weighting	Concept 1	Concept 2	Concept 3
Maintenance	0.045	6	4	2
Size-Restriction	0.015	5	2	5
Weight	0.106	5	2	2
Control Stability	0.167	4	6	2
Aesthetic	0.091	5	2	5
Material Cost	0.076	4	4	4
Manufacturability	0.136	4	4	4
Reliability	0.152	6	4	2
Noise	0.000	4	2	6
Unusable-Rotor	0.061	4	2	6
Transition Capability	0.030	5	5	2
Hover Efficiency	0.121	4	6	2
Total Score:	4.64	4.06		2.98

As can be seen in the *Table 2.2*, Concept-1 comes first with 4.64 points, followed by Concept-2 with 4.06 and Concept-3 with 2.98. As a result of it, the winning concept was a 3-rotor design, where the front two rotors can tilt and the rear rotor is active only during vertical take-off and landing. An example for the winner concept is shown in *Figure 2.3*. In following part of the design, further research on this concept was conducted in more detail. Control stability, hover performance and reliability are particularly important factors in the selection of the concept. In addition, the transition capability and the reduced number of unusable-rotors are also among the reasons for the victory of the concept.

In the later stages of the design process, more detailed analyses were carried out on the winning concept. Within the scope of these analyses, the performance of the propulsion system in different flight modes was evaluated. In addition, factors such as structural strength and dynamic stability, which ensure the long life and safe operation of the design, were also evaluated in detail. In this process, various optimisation and iteration studies were carried out to increase the suitability of the concept for different flight scenarios and to improve flight capability.

2.3. Detailed Design and Analysis

VTOL which is an efficient combination of two types of flying vehicle, flies as a fixed wing on majority of its flight time. It was decided to design a fixed wing vehicle that can operate stably, and then construct the tri-copter frame on the fixed wing aircraft. The reason behind the decision is that fixed wing aircrafts have more inflexible design parameters such as wing length, location of the CoG (Centre of Gravity), AoA (Angle of Attack) of wing etc. On the other hand, it is relatively easy to adapt rotary-wing aircrafts to different frame designs, and they provide a wider range for the specification of design parameters.

The most important part of the fixed wing vehicles is their wings which produce lift to keep the aircraft on-air and a significant portion the drag. For this reason, the wing design is considered as the most prioritised stage in the design process of the aircraft. The aspect was taken into account in the progress of the project and it was aimed to select the airfoil that will meet to the design criteria of the vehicle. Therefore, airfoils commonly used in commercial RC (Radio-Controlled) aircrafts were surveyed, and it was found three profiles that stand out with their differing advantages in application. These are NACA-6412, NACA-4412 and NACA-2412; these airfoils are shown in the *Figure 2.6*.

National Advisor Committee for Aeronautics (NACA) is an organisation founded in the USA in 1915 and conducting aeronautics research. The aerodynamic surface shapes developed and tested by the organisation, whose name has changed to NASA, are called NACA airfoils. [15] Each digit in NACA 4-digit airfoils refers specific characteristic of the airfoil. First digit refers maximum camber as percentage of the chord length, second digit refers to location of maximum camber with respect to leading edge and last two digits refer maximum thickness of the wing profile as percentage of the chord length. [16]

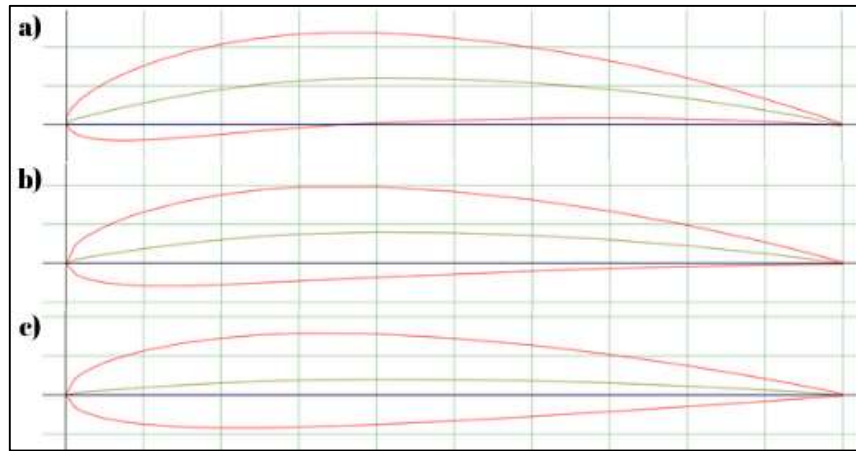


Figure 2.6 Commonly Used Airfoils: (a) NACA-6412; (b) NACA-4412; (c) NACA-2412.

The airfoiltools.com website was used to make comparative investigation of the selected airfoils. This web tool plots α (Angle of Attack) dependent variations of C_L (Lift Coefficient), C_D (Drag Coefficient), C_m (Moment Coefficient) values of the airfoil for a certain Re (Reynolds number). As seen in the *Figure 2.7*, polar diagrams are generated for $Re=100.000$. NACA-6412 has a high C_L value. NACA-2412 has a lower C_D value at 0-5 degrees, which is the AoA of operation. NACA-4412 has intermediate values in all graphs, but it also can be an optimal option for different manufacturing techniques such as balsa spar-rib construction thanks to its semi-linear bottom line.

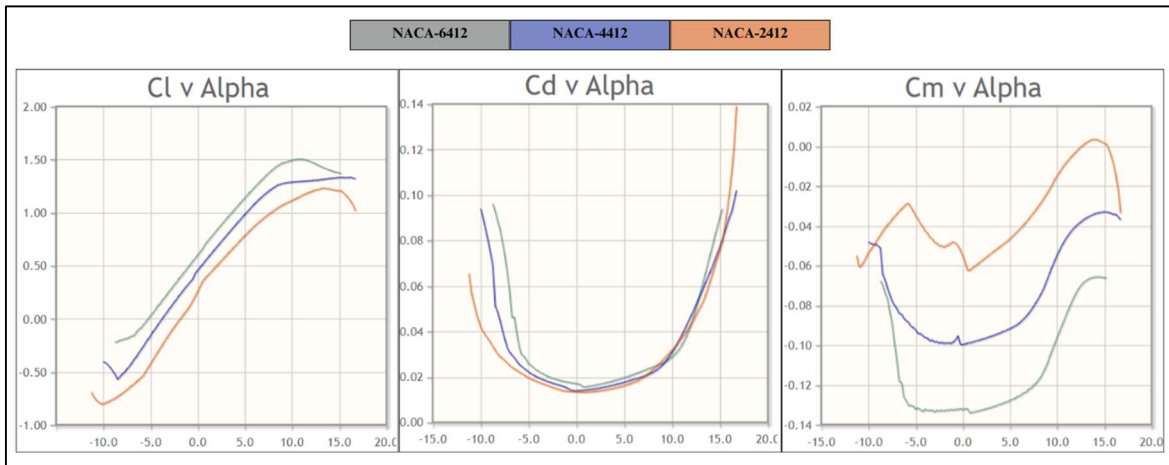


Figure 2.7 Polar Diagrams of Airfoils ($Re=100.000$).

The next stage is to design a wing that can generate enough lift to compensate for the expected take-off weight at lengths and speeds within the design limitation. The wing must produce at least 15N lift force to balance minimum take-off weight at a maximum speed of 13m/s and its length must be in the range of 1300-1500mm. XFLR5, a numerical aircraft analysis and fixed wing design software, was used for this purpose.

XFLR5 is a software developed specifically for model aircraft, unmanned aerial vehicles (UAV) and small-scale fixed-wing vehicles. The program is capable of both 2D aerodynamic and 3D numerical analysis. In wing design, XFLR5 is useful with its three-dimensional analysis capability. Using the panel method, aerodynamic properties of the wing such as lift, induced drag and moment can be computed. 3D Panel Method is ideal for evaluating the performance of wings with different geometries. Furthermore, the user can determine the aerodynamic centres of the wing and stabilisers and examine the effect of in-flight moments on stability.

The process was carried out through iterations and the optimal wing geometry was tried to be obtained. The primary focus was on the lift force, while the total drag force and pitching moment were also considered. 3D Panel Analysis method was used and constant lift analysis condition was applied. 1.5 kg of point mass is located at quarter chord length from the leading edge. The algorithm calculates the minimum speed required for the wing to generate sufficient lift at different AoA values, and the software stores the operation points. Total of 6 iterations were performed. Some significant geometric parameters of the wing designs and their required minimum speed obtained from the analysis are shown in *Table 2.3*.

Table 2.3. Geometric Parameters and Analysis Results of Design Iterations.

Parameters	1 st Iteration	2 nd Iteration	3 rd Iteration	4 th Iteration	5 th Iteration	6 th Iteration
Wing Span [m]	1.300	1.300	1.500	1.500	1.500	1.640
Wing Area [m ²]	0.191	0.210	0.251	0.251	0.252	0.266
Airfoil (NACA)	N-4412	N-4412	N-4412	N-6412	N-6412	N-6412
Root Chord [m]	0.230	0.230	0.230	0.230	0.250	0.250
M.A.C. [m]	0.191	0.191	0.191	0.191	0.191	0.186
Wing Load [kg/m ²]	7.843	7.143	5.970	5.970	5.980	5.726
Tip Twist [°]	0	0	0	0	-3.0	-3.0
Aspect Ratio	8.837	8.048	8.995	8.955	8.970	10.10
Tilt Angle [°]	2.0	2.0	2.0	2.0	3.0	3.0
Cruse Speed [m/s]	18.75	17.37	15.23	13.22	13.16	12.77
Stall Speed [m/s]	12.2	11.28	9.854	9.249	9.202	8.923

In the first iteration, the rough dimensions of the concept vehicle were taken as the initial values. Since the minimum velocity to produce sufficient lift was outside the design limits, it is decided to increase the wing area in the second and third iterations. At the fourth iteration, it was realised that a higher C_L airfoil was needed. Therefore, the profile changed to NACA-6412 which offers almost 20% higher C_L at 2° AoA (See *Figure 2.7*). At the fifth iteration, the tilt angle of the wing is increased to 3° with negative tip twist angle of 3° and the root chord was increased to compensate for the resulting lift. This type of negative tip twist is called wing washout, and it provides many benefits. Especially at high angles of attack, flow separation starting from the wing tips is observed and it causes a dangerous situation, loss of aileron control [17]. The washout is useful technique to prevent it. Additionally, it reduces the rotational moment generated by the wing. Final iteration is completed with the addition of winglets. They are beneficial for reducing the wing tip vortices and cause little improvement of the lift force. Also, in all design, sweep angle is applied to keep maximum thickness position of the airfoil as straight line along the wing. It is the line where we will position the spar tube that will provide the strength of the wing, and a straight maximum thickness line gives the flexibility in determination of the tube diameter.

Final geometry of the wing is given in *Appendix A*. For a more comprehensive performance evaluation, 3 different analyses are performed for final iteration. Those are Constant AoA vs. Velocity which computes generated forces, Constant Lift Force (15N) vs. AoA which computes required air speed and Constant Velocity (12.8 m/s) vs. AoA which computes generated forces. Drag and lift forces versus velocity and α is plotted and polar are shown in *Figure 2.8*.

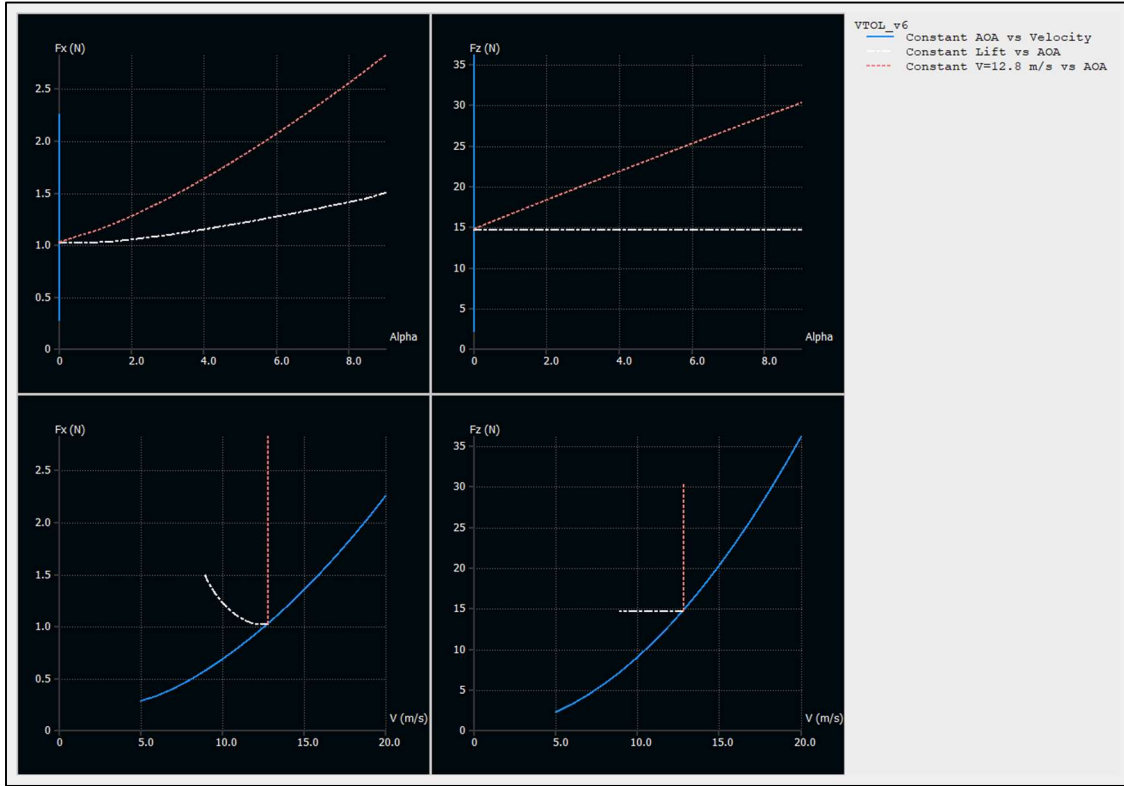


Figure 2.8 Results of Force Analysis of the Final Wing Design.

After the wing design process, the aircraft needed a tail. The tail is used to compensate the moments of the aircraft and responsible for generating pitching and yawing movements by affecting resulting moments of the aircraft. Another important concept for fixed-wing aircrafts is Tail Volume coefficient. It is a non-dimensional scale of tail effectiveness. It can be easily derived from span-wise Moment Equilibrium of the aircraft [18].

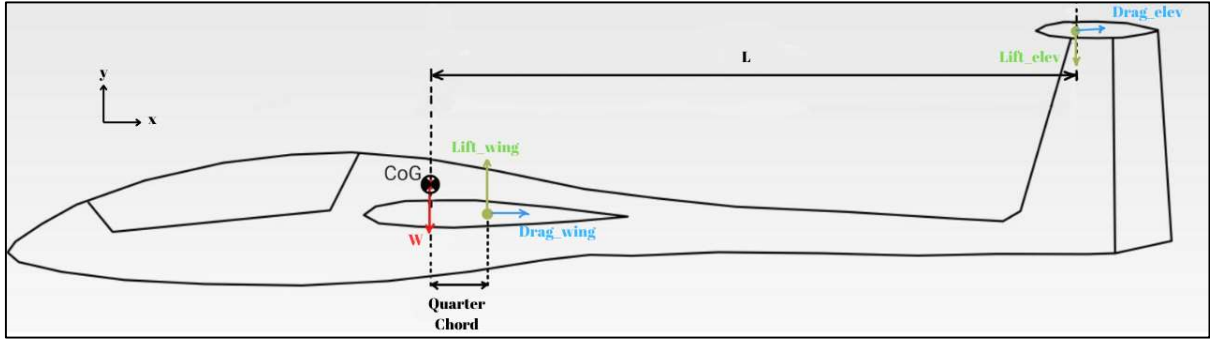


Figure 2.9 Span-wise Free-Body Diagram of the Aircraft.

During calculations C_m of the horizontal stabiliser is neglected, and it is assumed that y-axes of the CoG is such that the moments produced by drag forces of the wing and the horizontal stabiliser cancel each other. Also, x-axes position of the CoG is located on quarter-chord length behind from the leading edge. FBD of the aircraft is shown on the *Figure 2.9*.

$$F_{Wing} = q \cdot C_{L,wing} \cdot A_{wing} \quad \text{and} \quad F_{elev} = q \cdot C_{L,elev} \cdot A_{wing}$$
Eq. 2.1

Lift forces calculated by *Eq. 2.1* where q is dynamic pressure and A is area of a member. The total moment about the CoG is:

$$\sum M = \frac{1}{4} \cdot L_{chord} \cdot F_{wing} - L \cdot F_{elev} = 0$$
Eq. 2.2

The moment caused by the lift at quarter-chord of the wing is also calculated by this:

$$M_{wing} = q \cdot C_M \cdot M.A.C \cdot A_{wing} = \frac{1}{4} \cdot L_{chord} \cdot F_{wing}$$
Eq. 2.3

By implementing *Eq. 2.1* and *Eq. 2.3* to total moment equation (*Eq. 2.2*) it gives:

$$C_{m,wing} = \frac{L \cdot A_{elev}}{M.A.C \cdot A_{wing}} \cdot C_{L,elev} = TV \cdot C_{L,elev}$$
Eq. 2.4

The Tail volume constant is calculated by the *Eq. 2.4* where *M.A.C.* is mean aerodynamic chord length and L is lever length of the horizontal stabiliser. For sailplanes, TV for horizontal stabiliser is between 0.5 and 0.7, and during design process of the tail, it was worked in the interval [18]. A horizontal stabiliser was designed with aspect ratio of 3.5, and it was converted a V-Type tail design without changing its projected area. Some geometric properties of the V-Tail stabiliser can be seen in *Table 2.4*. Technical drawings and detailed dimensions of the tail is provided in *Appendix B*.

Table 2.4 Geometric Properties of the V-Tail Stabiliser.

P. Stabiliser Span [m]	0.500
P. Stabiliser Area [m^2]	0.06
Airfoil (NACA)	N-0012
Root Chord [m]	0.180
Tip Chord [m]	0.100
M.A.C. [m]	0.152
Tilt Angle [°]	-3.0
Tail Volume	0.61
Dihedral Angle [°]	35.0
Lever Arm, L [m]	0.650

Another important concept for the tail design is consideration of the static stability. XFLR5 is able to compute the total moment coefficient of the vehicle. There are two graphs in XFLR5 that should be examined to verify static stability. C_M vs. α graph must have negative slope, it means that the increasing α creates negative pitching moment that will bring the vehicle back to its equilibrium. At equilibrium α , the wings could generate sufficient lift to keep the vehicle on air. As seen in *Figure 2.10*, the aircraft can fulfil both condition at 13.6 m/s with generated 16N lift. Although the velocity is slightly out of the design margin, this margin can be acceptable.

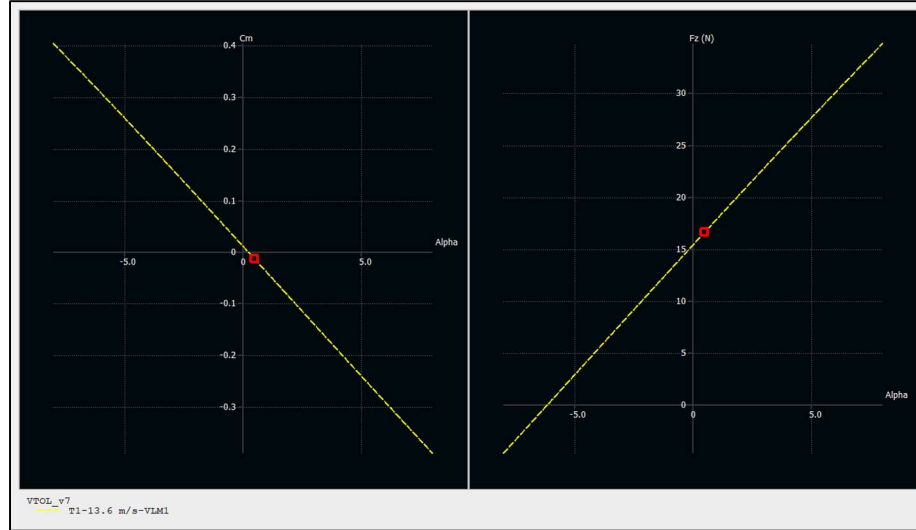


Figure 2.10 Constant Velocity (13.6 m/s) vs. AoA Analysis Results of the Aircraft with V-Tail.

After that stage, the 3D design and dynamic stability analysis were carried out simultaneously. The main reason behind this was the fact that the moment of inertia of the vehicle was required for dynamic stability analysis. SolidWorks had been used as the 3D design software. The vehicle was designed as an outer shell and an internal structure to support the shell. Since additive manufacturing was preferred for production, designing complex internal structure will not cause any major production problem. It was aimed to overcome the disadvantage of low-strength property of the FDM printing technique by utilising pre-produced composite materials in sections requiring strength.

The dimensions of the spar tube to be selected to reduce the deflection and increase the overall strength of the wing were determined by numerical analysis. In order to simplify calculation, internal structure of the wing was not taken into account, and only the wing shell and composite tube were included in the analysis. The second moment of area of the wing profile was computed by the SolidWorks. I_{Shell} for a profile with 250mm of chord length and 0.8mm of thickness equals to 55082 mm^4 . It was observed that I_{Shell} is proportional to the cube of the chord length with a multiplication constant of 3.53×10^{-6} . The distance between neutral axis of tubular section and neutral axis of the total section is observed as proportional to the chord length with a multiplication constant of 1.22×10^{-2} . Similarities are checked for 5 different section of wing profile and multiplication constants are given in *Table 2.5*.

Table 2.5 The Geometric Properties and Multiplication Constants of Wing Section with Different Chord Lengths.

Chord Length [m]	I_{Shell} [m^4]	D_{trans} [m]	C_1 [m]	$C_{D,T}$
0.250	55082×10^{-12}	3.06×10^{-3}	3.52×10^{-6}	1.22×10^{-2}
0.220	37568×10^{-12}	2.68×10^{-3}	3.52×10^{-6}	1.22×10^{-2}
0.200	28242×10^{-12}	2.44×10^{-3}	3.53×10^{-6}	1.22×10^{-2}
0.190	24213×10^{-12}	2.30×10^{-3}	3.53×10^{-6}	1.21×10^{-2}
0.180	20645×10^{-12}	2.18×10^{-3}	3.54×10^{-6}	1.21×10^{-2}

XFLR5 is able to compute bending moment caused by the lift and drag, the results that cause maximum bending moment were exported to MATLAB. Since positions of the motors haven't yet been decided, the vertical point force generated by the propellers in vertical flight was assumed to be applied at the farthest point of the wing from the centre. The total Flexural Rigidity for a composite beam is derived below.

$$I_t = I_1 + nI_2, \quad n = \frac{E_2}{E_1} \quad [19]$$

Eq. 2.5

Where I_1 and I_2 are second moment of area about neutral axis of composite beams, and I_t is the equivalent second moment of area for entire beam made of a material with elastic modulus of E_1 . The Flexural Rigidity, D is calculated as;

$$D = E_1 I_t = E_1 I_1 + E_2 I_2$$

Eq. 2.6

And so on, the deflection of the wing is computed by using Eq. 2.7 and *cumtrapz* function of the MATLAB by applying boundary conditions where the deflection and its slope are equal to zero at the centre. MATLAB Code to compute the deflection is given in *Appendix C*.

$$\frac{d^2v}{dx^2} = \frac{M}{D} \quad [20]$$

Eq. 2.7

The maximum deflection is expected not to exceed 10% of the wing length, which is 80mm. Accordingly, a 500mm long CFRP tube with an inner diameter of 10mm and an outer diameter of 12mm was used as the spar tube. Since the CFRP tube is sold in 1 metre pieces, not exceeding 0.5 metres for each wing will reduce the cost. As seen in the *Figure 2.11*, the maximum deflection which located at wing tips is not exceed 25mm in horizontal flight. Although a higher deflection is emerged during vertical flight, the results are still within an acceptable level.

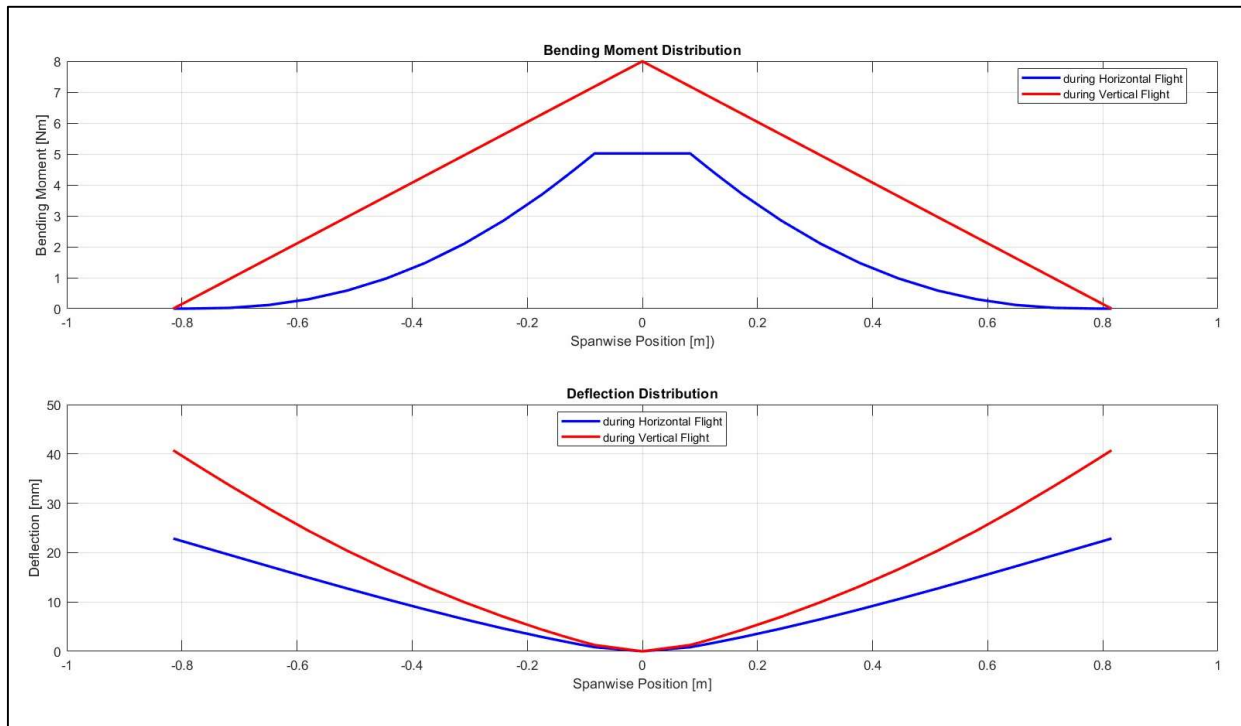


Figure 2.11 The Numerical Deflection Analysis Results.

The rough design was finalised taking into account the mentioned concepts. Moment of Inertias of the plane were exported from SolidWorks, and the battery, motors and other significant masses are added to XFLR5 as point masses. Thus, the inputs required for the stability analysis were roughly fed into the programme. During the analysis, the damping ratios and frequencies of the natural aerodynamic modes are computed as eigenvectors and eigenvalues by XFLR5. The real parts of these eigenvalues are related to the damping coefficient and their imaginary parts correspond the frequencies. The resulting eight modes can be divided into, four longitudinal and four lateral modes, some of which are symmetric.

The longitudinal modes are two symmetric Phugoid Modes and two symmetric Short-Period Modes. The phugoid is a long period oscillation of change in altitude, that is caused by the exchange of kinetic and potential energy and it is usually lightly damped. For our plane the damping ratio, ζ of this mode is computed to be 0.033 and the damped natural frequency is 0.896 Hz. Its duration could be several minutes for a stable aircraft and the settling time is nearly 1.5min for the aircraft [21]. Modal response is shown in right 4-graphs of *Figure 2.12*. The other longitudinal mode is the Short-Period mode. This mode is related to pitch rate and vertical displacement. It is usually high frequency and damped well. For the plane, the damping ratio, ζ of this mode is computed to be 0.553 and the damped natural frequency is 11.57 Hz. Its settling time is expected to be less than a second for a stable aircraft, it takes 0.6s stabilise for the aircraft [21]. Modal response is shown in left 4-graphs of *Figure 2.12*.

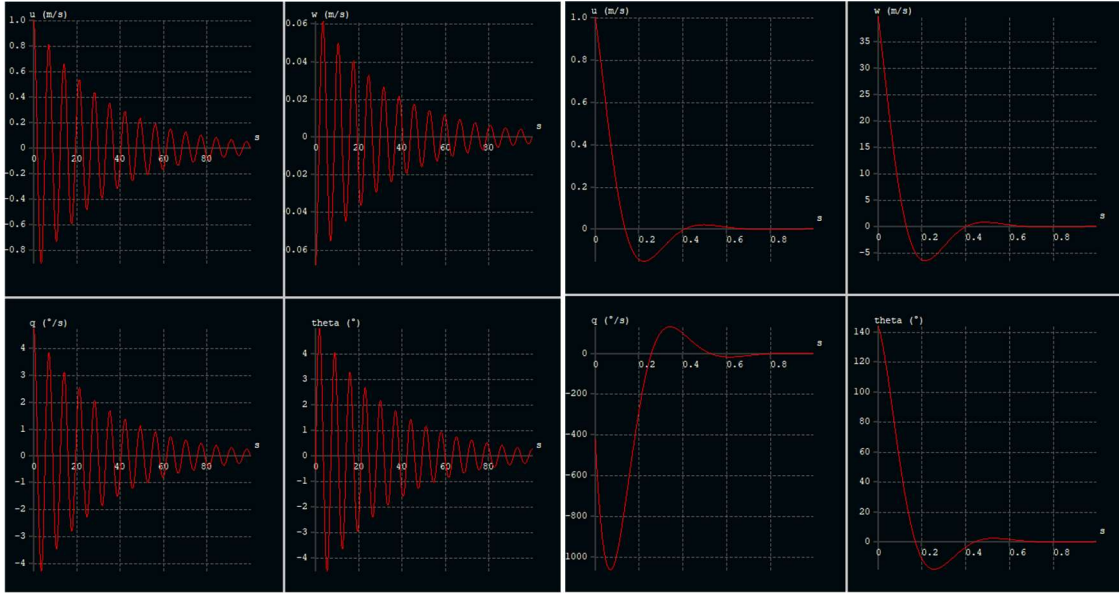


Figure 2.12 Longitudinal Modal Responses of the Vehicle: (Right-4) Phugoid Mode; (Left-4) Short-Period Mode.

The lateral modes are Spiral Mode, one Roll-Damping Mode and two symmetric Dutch-Roll Modes. The Spiral Mode is primarily a change in heading and it is a non-oscillatory and slow mode and it is usually unstable. This mode is also unstable for the plane as can be seen from the modal response in *Figure 2.13*. Although it is unstable in Spiral mode, it can be easily corrected by the pilot since it is very slow. For the plane, the doubling time is computed to be 4.23s and the task of stabilizing it was assigned to the flight controller. Flight controllers with flight control software such as PX4 or Ardupilot, can easily handle such stabilization operations. It also improves the controllability of the vehicle, offers easier flight modes for the pilot and can operate the vehicle in autonomous flight modes [22].

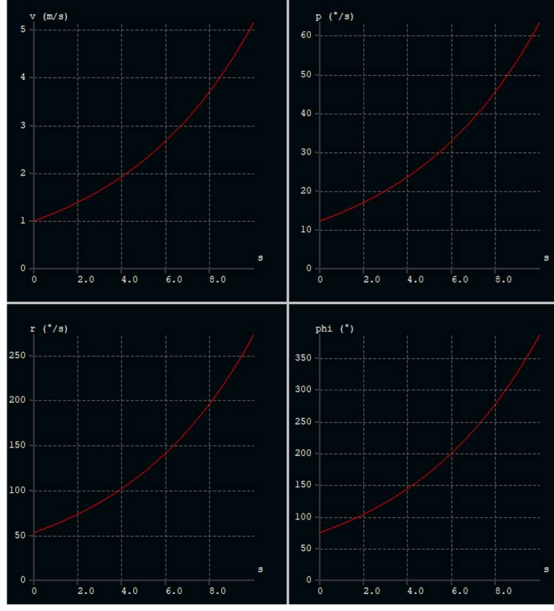


Figure 2.13 Spiral Mode Modal Responses of the Vehicle.

Another lateral mode is Roll-Damping which is related to a change in roll. This mode is non-oscillatory and usually fast. For our plane the halving time is computed to be 0.055s . The modal response of Roll-Damping mode is shown in right 4-graphs of the *Figure 2.14*. Lastly, there is the Dutch-Roll mode which is a combination of roll and yaw change with a 90° phase difference. Dutch-Roll mode is usually lightly damped. For the plane, the damping ratio, ζ of Dutch-Roll mode is computed to be 0.165 and the damped natural frequency is 4.22 Hz. Modal response is shown in left 4-graphs of the *Figure 2.14*

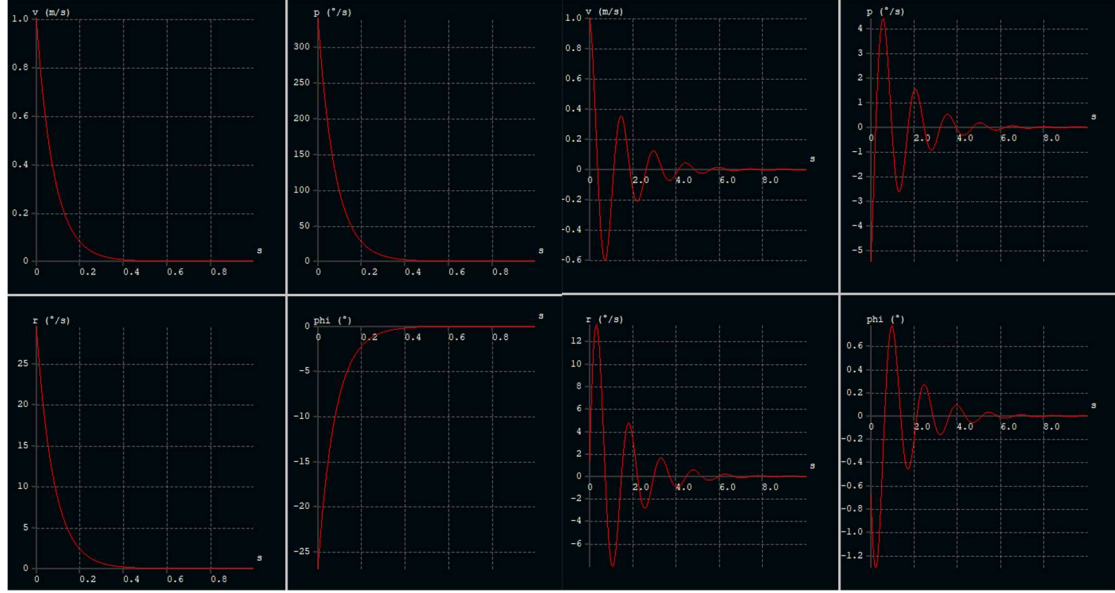


Figure 2.14 Lateral Modal Responses of the Vehicle: (Right-4) Roll-Damping; (Left-4) Dutch-Roll Mode.

One of the important parameters for a reliable vertical flight is the thrust-to-weight ratio. It is calculated as the maximum thrust obtained from the propellers multiplied by the number of rotors divided by the weight of the vehicle. While thrust-to-weight ratio is accepted in the range of 2-4 for quadcopters, it has been found that the range of 1.5-3 is recommended for VTOL vehicles that perform vertical flight for a short period of their flight. Considering a 3-rotor VTOL with a maximum take-off weight of 2 kg, the motors are expected to generate 1 to 2 kg-force static thrust. After the market research, Emax RS2205S-2300Kv model BLDC motors were selected. They are

able to produce 1281 gr-force thrust with 3 blade 5045 propellers and they consume maximum of 33A current with nominal voltage of 16V. With this configuration, the thrust-to weight ratio is calculated as minimum of 1.92. Another market research was also conducted out for servo actuators to be used in the tilt mechanism. It was decided that Emax ES09MD Dual-Bearing servo actuators are suitable for the system. They have 2.6 kg-force.cm stall torque with angular speed of 6.55 rad/s at operating voltage of 6V. Thanks to dual-bearing design of output shaft, they can withstand not only twisting but also bending moments.

As the plane has three rotors, two at the front and one at the back; their positions must be designated. In the designation of rotors, there are several important criteria. In the vertical thrust, it is desired that the rotors should produce the same thrust. That requires proper placement of rotors with respect to centre of gravity. As Eq. 2.8 shows, the position of back rotor is the double distance of front rotors with centre of gravity in z axis. As the propellers produces vertical thrust, the thrust should not interfere with either the wing or the fuselage. The diameter of 3 blade 5045 propellers is 127mm. With that size and the dimension of plane in account, the positions of front and back rotors are located 160mm and 320mm away from the centre of gravity. The other important criterion for the designation is the distances between rotors. To achieve optimized balance and stability, the rotors are placed equidistant from each other. That allows symmetrical thrust distribution and more stable control. With that the designation of rotors are finalized as shown in *Figure 2.15*.

$$\sum M_x = 0 , \quad F_{back} = F_{front} , \quad F_{back} z - 2 \times F_{front} z = 0$$

Eq. 2.8

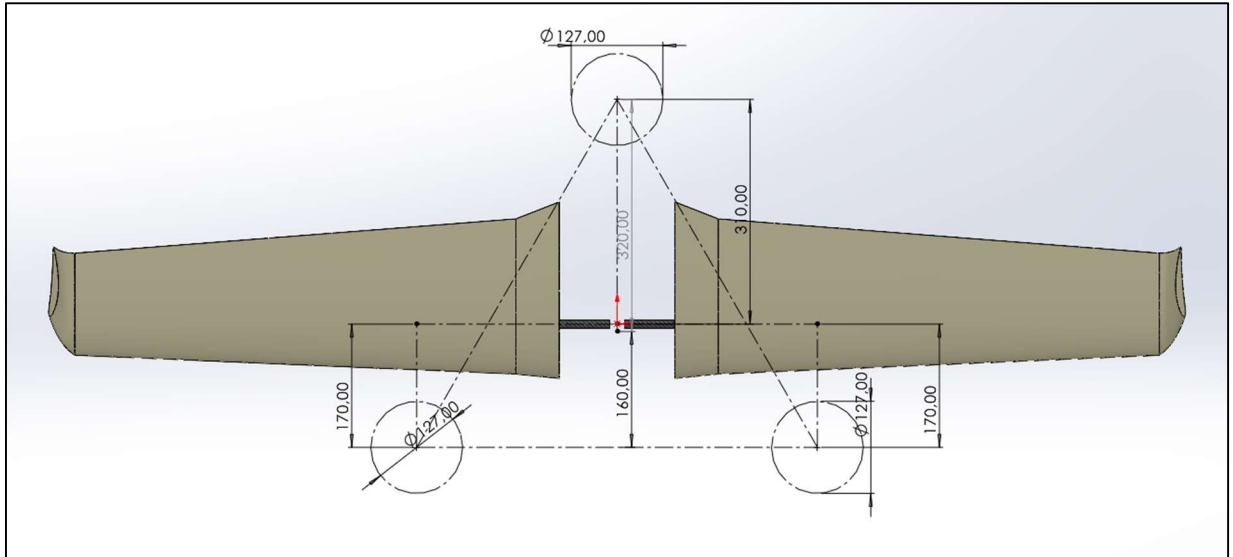


Figure 2.15 The Designation of Rotor Positions.

After the positions and necessary mechanism are determined, tilt mechanism must be designed accordingly. The positions of the BLDC motors are sufficiently enough from the wings. That brings additions in the wings. According to these considerations, it is decided that the servo actuators can be directly connected to the BLDC motors. That simplifies the tilting mechanism design and allows more stable structure. The servo motors are located in the inside of the support addition. Therefore, the design of these support units is based on the size of servo motors, while maintaining structural integrity and strength. The connection between servo motors and BLDC motors are designed in a way that the thrust produced by the propellers does not create any moment in the rotating axis of servo motors. That lowers the force applied on the servo motors. The finalized design of tilting mechanism is shown in *Figure 2.16*.

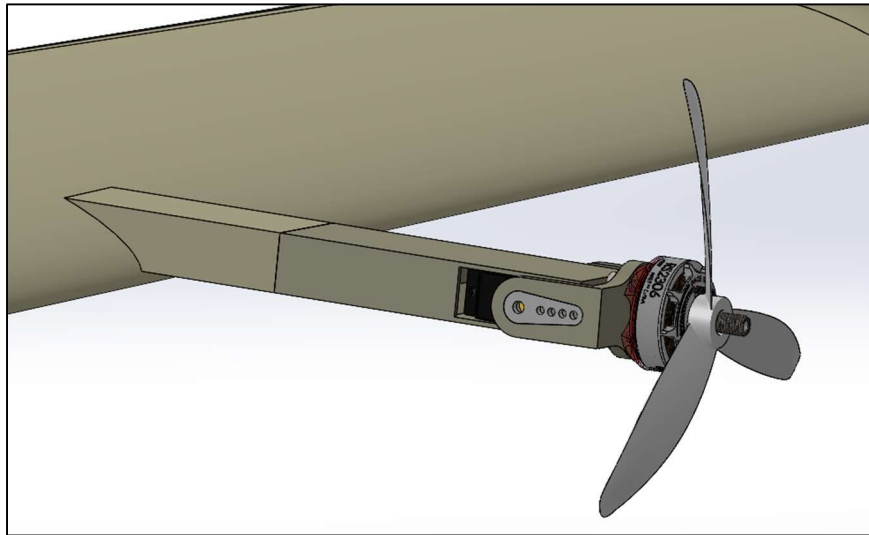


Figure 2.16 The Tilting Mechanism.

The next stage of the design is the structural analysis of the wing members. In the process, the finite element analysis software Ansys was used. The loads acting on the wing during both horizontal and vertical flights were applied and wing mounting joints were established, and the results were examined for both loadings. Since the materials produced with the 3D printer exhibit orthotropic behaviour, it wouldn't be a reasonable approach to assign isotropic materials from the material library. Therefore, academic article research was carried out, and a paper that has an experimental approach to mechanical properties of 3D printed PLA samples was found. The mechanical properties of the material were taken from this article and entered into the software. Mechanical properties such as shear yield stress, Poisson's Ratio which are not mentioned in the article were assumed to be the same as raw PLA. Young's Modulus of FDM printed PLA material is 2251.4 MPa in axis parallel to layers and 1951.5 MPa in axis perpendicular to layer lines for 0.2mm layer heights. [23] From the analysis; displacement, equivalent Von-Misses stress and safety factor according to the yield strength of the assigned material were obtained.

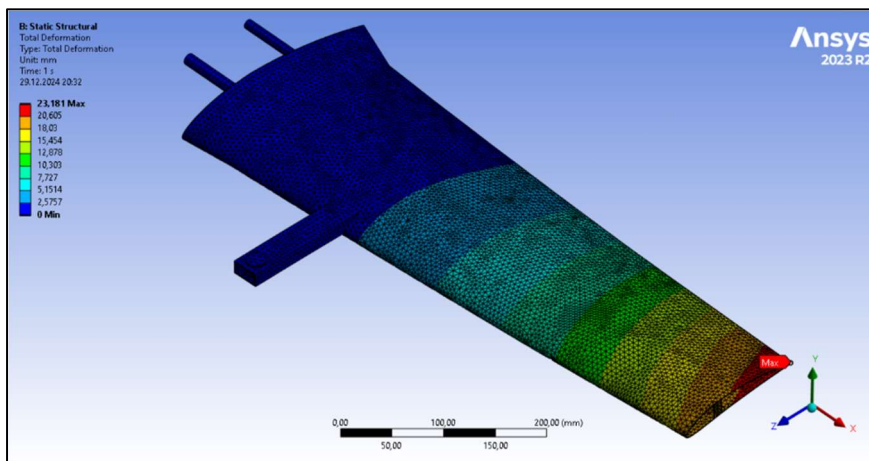


Figure 2.17 Wing Total Deformation Results of FEA for Horizontal Flight.

As can be seen in the *Figure 2.17*, the maximum deflection during horizontal flight occurs at the wing tips, as expected. Also the maximum deflection was consistent with the results of the numerical analysis. The maximum deformation found to be 25mm in the numerical analysis was observed as 23mm in the FEA results. In addition, the maximum elastic deformation in vertical flight was observed as 3.7mm at the end of the tilt mechanism where the motors are attached. It can be seen in *Figure 2.18*. The deflection was kept so low thanks to the dense interior infill applied to the extension arm and wing contact surface.

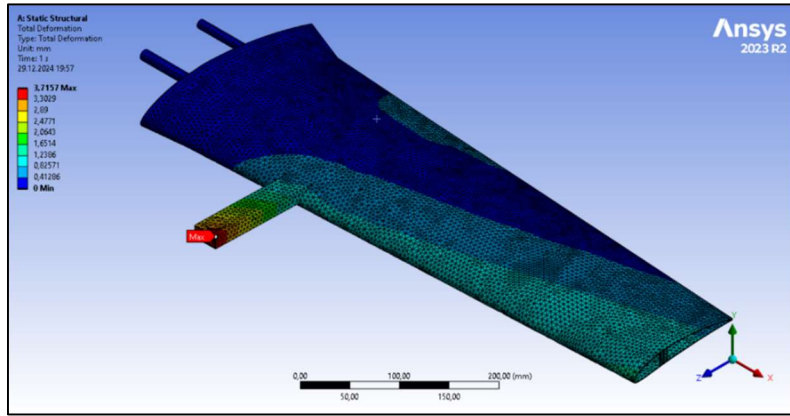


Figure 2.18 Wing Total Deformation Results of FEA for Vertical Flight.

The Equivalent stress on the wing during horizontal flight was found to be concentrated on the carbon spar pipe. Therefore, iso-clipping is performed for stresses below $5MPa$ for better visualisation of stress concentration points which are marked in both *Figure 2.19* and *Figure 2.20*. The maximum equivalent stress is found to be $57.8MPa$ for horizontal flight. The stress development area on the spar pipe which is coloured red-orange lays between $50-58MPa$ range. Both are shown in *Figure 2.19*.

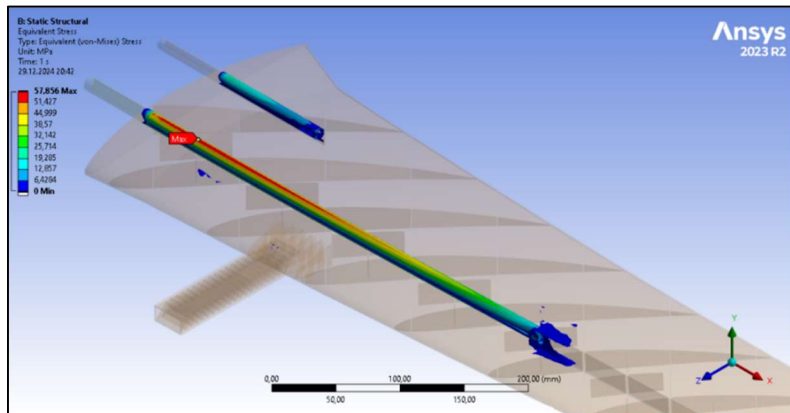


Figure 2.19 Equivalent Stress on the Wing Results of FEA for Horizontal Flight.

For vertical flight loads were applied at the tip of the arm, and maximum equivalent stresses were found lower than the horizontal flight results (See *Figure 2.20*). It is as expected because load is $12N$ which is maximum static thrust can be generated by rotors and also moment arm is shorter than the horizontal flight load. The stress development starting from the contact point of the arm and wing to tip of spar pipe is shown in *Figure 2.20*.

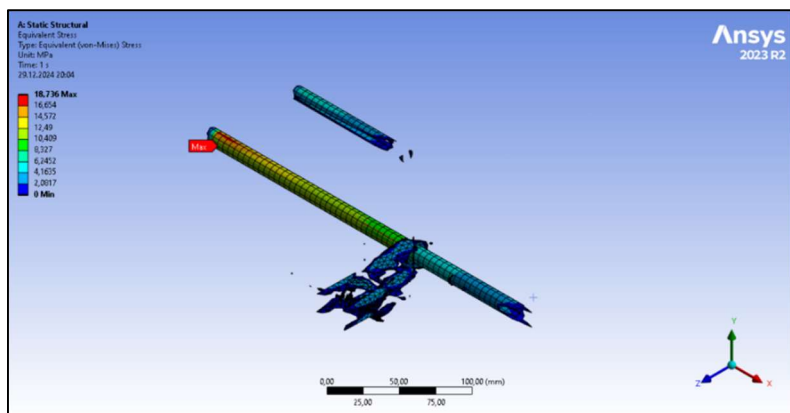


Figure 2.20 Equivalent Stress on the Wing Results of FEA for Vertical Flight.

Even if the applied load of 19N at wing tip which develops higher bending moments than generated by the lift at all points of the wing, resulting stresses are way lower than the materials yield stresses. Safety factor with respect to yield stress of the materials was also provided by Ansys. Under horizontal flight loads; minimum safety factor is 1.96 for structures made of PLA, and minimum safety factor is calculated as 3.94 for carbon structures which are spar pipe and back mounting pipe. Under vertical flight loads; minimum safety factor is 1.72 for structures made of PLA, and minimum safety factor is calculated as 11.4 for carbon structures which are spar pipe and back mounting pipe.

At the end of the design, it was intended to evaluate the performance of the aircraft. For that purpose, the power consumption of the aircraft in horizontal and vertical flight had to be calculated with reasonable assumption and formulas. The height at which the transition to horizontal flight from vertical flight is called the transition height and the required times to smooth transition is called the transition time. In Ardupilot, the flight control software, the default value of transition height is $30m$, and the default value of transition time is $7s$. The vertical speed up value for autonomous modes is set to be $1m/s$ as default. With these parameters, it takes $30s$ to reach the transition height. It is assumed that the power consumption during transition is approximately equals to the power consumption of the vertical flight.

Generated drag during vertical ascending is assumed to be 20% of the aircraft weight which is $19.62N$. The force required to be generated by the rotors to maintain static equilibrium is

$$\frac{19.62[N] \cdot 1.2}{3} = 7.848 [N]$$

Eq. 2.9

Dynamic thrust generated by a propeller with diameter of $d = 5\text{inch}$, pitch of $p = 4.5\text{inch}$ and rotational speed ω in RPM can be calculated with Eq. 2.10. Simplified form of the equation is given, and it was derived by Gabriel Staples.

$$F [N] = 1.306 \cdot 4.392499 \cdot 10^{-8} \cdot \omega \cdot \frac{d^{3.5}}{\sqrt{p}} (4.23333 \cdot 10^{-4} \cdot \omega \cdot p - V_0) \quad [24]$$

Eq. 2.10

Where V_0 is propeller axial velocity in m/s . During vertical flight, propeller axial velocity equals to $1m/s$. After solving Eq. 2.9 and Eq. 2.10 together, it was concluded that required angular velocity of propeller is approximately 23600 RPM . When the manufacturer data sheets are analysed, it can be seen that the motor rotating at this angular speed consumes approximately $355W$ electrical power. Total energy consumption is calculated as $1065W$ during vertical flight.

The aircraft experiences a drag force of $2.5N$ at cruise speed. It is sum of parasitic and induced drag forces generated by the wing and the elevator. XFLR5 is capable of compute these forces. Drag force experienced by the fuselage could not be calculated. It is assumed that fuselage drag equals to what rest of the aircraft experiences. So that, total drag is equals to $5N$. The force required to be generated by the rotors to maintain static equilibrium is $2.5N$ for each tilting rotor.

By using equation Eq. 2.10 where V_0 equals to cruise speed which is $13.6m/s$, it was concluded that required angular velocity of propeller is approximately 17200 RPM . The motor rotating at this angular speed consumes approximately $145W$ electrical power. Total energy consumption is calculated as $290W$ during vertical flight.

The battery planned to be used is a 4S Li-Po battery with a nominal voltage of $14.8V$ and a capacity of 4500mAh . It can storage $71.1Wh$ energy, and 80% of it can be used without damaging the battery. The aircraft consumes $21.9Wh$ energy during take-off, landing and transition. With the remaining $35Wh$ of energy, the aircraft can perform $7.2min$ of horizontal flight. With a total flight time of 8.5 minutes, the vehicle has a range of $5.9km$.

3. Manufacturing Process

3.1. Selection of Materials

As the functional requirements suggested, the manufacturing is supposed to be manufactured by mostly additive manufacturing. In the 3-D manufacturing at commercial level, there are several types. The most common one is 3-D manufacturing with filaments. Filaments are chosen because of their decent mechanical properties, ease of manufacturability, and cost advantages. For the project, PLA and ABS type filaments are used. [25]

Polylactic Acid (PLA) is a biodegradable polyester made from renewable sources like corn starch. Compared to other filaments, it exhibits lower glass transition temperature between 60 and 65 degrees Celsius and a melting range between 150 and 180 degrees Celsius. PLA can be manufactured with both unheated and heated beds which makes it very convenient material for printing. Currently, its price is very affordable range in the market. Its relatively satisfactory strength and other mechanical properties are quite suitable for the project. Most of the plane parts including tail, fuselage and wing are manufactured with PLA. [26]

The other key filament is ABS, also known as Acrylonitrile Butadiene Styrene. It is a petroleum-based copolymer with higher glass transition temperature around 105 degrees Celsius. Its printing temperatures range from 220 to 250 degrees Celsius which is also manufacturable for most of the printers. Although it has better toughness compared to PLA, the main reason for the selection is its temperature resistance. For the project, its mainly used in places where heat can increase above the glass transition temperature of PLA. [27]

Table 3.1 Mechanical Properties of PLA and ABS.

Properties	PLA	ABS	Unit
Glass Transition Temperature	55-65	~108	°C
Melting Temperature	150-180	~200	°C
Tensile Strength	50-70	30-50	°C
Young's Modulus	3.0-3.5	2.0-2.5	GPa
Impact Resistance	0.6-1.2	3.5-5.0	kJ/m ²

As shown in *Table 3.1*, the values are given in the range. That cause from the facts like material variability, orthotropic effects in the filaments. In 3-D printing, orthotropy results from in Fused Deposition Modelling. In this process, thermoplastic filament is heated and extruded through a nozzle. With that, the part is produced layer by layer. Consequently, the filament exhibits higher strength and stiffness along the extrusion direction, while it has lower strength and stiffness between the layers. [28]

The other structural material is glass fibre resin reinforced polymer (GFRP) tubes. GFRP tubes made from glass fibres embedded in a thermosetting epoxy resin. It has very excellent tensile stiffness and a tensile strength around 600-1400 MPa with a sufficiently low density around 1.8-2.0 g/cm³. In the project, GFRP tubes are used as internal support in the wings and a connection unit between fuselage and tail. For the wings, it is found that the stresses can cause high stress due to bending that can create fractures. Therefore, the use of GFRP tubes is chosen to overcome bending. Additionally, it enables a certain level of stability by making wing stiffer. After the market research and technical research, it is decided that a tube with 14mm outer and 12mm inner diameter is sufficiently rigid for the wings. For the tail pipe, the tube with 12mm outer and 10mm inner diameter is chosen. [29]

3.2. Selection of Manufacturing Processes

The parts of the vehicle are produced by 3D Printing, an additive manufacturing technique. Creality's Ender3-S1 open-frame printer (See the **Figure 3.1** Ender3-S1 3D Printer.*Figure 3.1*), which was decided to be suitable for this application, was used. The printer has a print volume of 220x220x280mm, so the designed vehicle is divided into parts to fit this volume. Thanks to the automatic bed levelling feature of the printer, it has shown successful first layer performance even on parts with low adhesion surface to the plate. The printer has a direct drive extruder which minimised the elastic elongation of the filament during ejection and retraction, and it was able to print with consistent wall width. It resulted in an almost flawless surface finish on the printed parts.



Figure 3.1 Ender3-S1 3D Printer.

Three different software were tried as the slicer software, these are Cura, Prusha Slicer and Orca Slicer. Prusha Slicer was preferred because of its success in hiding seam marks. User interface of the Prusha Slicer is shown in *Figure 3.2*. The PLA filament was printed at a nozzle temperature of 210 °C and a bed temperature of 60 °C, while the cooling fan was operated at full power. All parts are printed at the 40mm/s print speed recommended by the printer manufacturer. In order to prevent problems such as warping or removing from the table, the brim feature has been enabled on all printed parts and 5mm brim has been added.

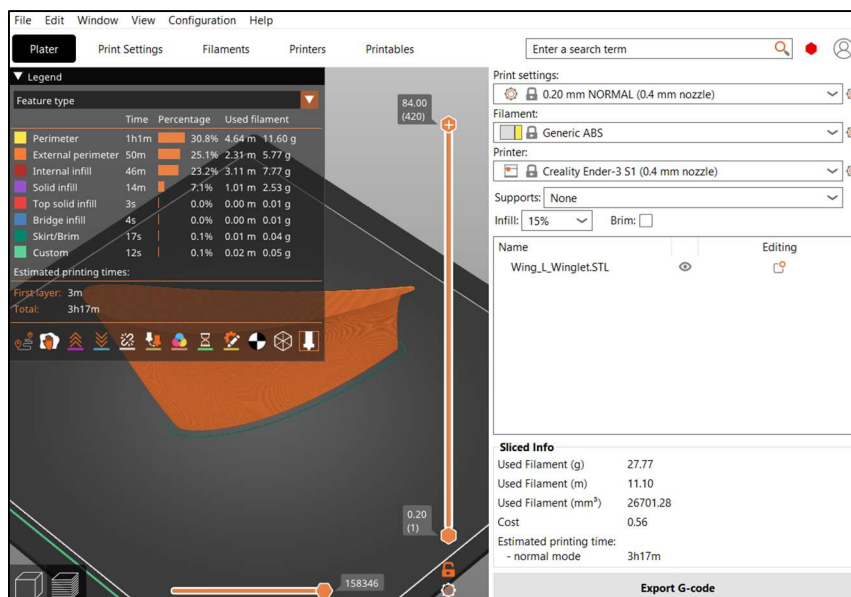


Figure 3.2 Prusha Slicer User Interface.

Table 3.2 Manufacturing Time and Weight of the Printed Parts of the Vehicle.

Title of the Part	Print time	Used Material	Infill	Wall Line Count	Support Requirement
Wing_L_P1	12h 13min	90.24g	By Design	By Design	No
Wing_R_P1	12h 13min	90.24g	By Design	By Design	No
Wing_L_P2	12h 19min	89.72g	By Design	By Design	Yes
Wing_R_P2	12h 19min	89.72g	By Design	By Design	Yes
Wing_L_P3	8h 55min	65.79g	By Design	By Design	No
Wing_R_P3	8h 55min	65.79g	By Design	By Design	No
Wing_L_P4	7h 59min	57.26g	By Design	By Design	No
Wing_R_P4	7h 59min	57.26g	By Design	By Design	No
Wing_L_Winglet	2h 15min	17.08g	2% (Gyroid)	2	No
Wing_R_Winglet	2h 15min	17.08g	2% (Gyroid)	2	No
Wing_L_Ailerons	4h 27min	20.12g	3% (Gyroid)	1	No
Wing_R_Ailerons	4h 27min	20.12g	3% (Gyroid)	1	No
Wing_L_ServoCap	32min	4.43g	15% (Grid)	3	No
Wing_R_ServoCap	32min	4.43g	15% (Grid)	3	No
Arms	2h 53min	25.39g	15% (Grid)	3	No
Vtail_L	10h 15min	73.97g	By Design	By Design	No
Vtail_R	10h 15min	73.97g	By Design	By Design	No
Vtail_Mid	2h 45min	26.23g	15% (Gyroid)	3	Yes
Ruddervator_L	2h 33min	11.89g	3% (Gyroid)	1	No
Ruddervator_R	2h 33min	11.89g	3% (Gyroid)	1	No
Vtail_L_ServoCap	29min	4.08g	15% (Grid)	3	No
Vtail_R_ServoCap	29min	4.08g	15% (Grid)	3	No
Fuselage_P1	5h 09min	37.23g	By Design	By Design	No
Fuselage_P2	13h 34min	97.01g	By Design	By Design	No
Fuselage_P3	14h 28min	100.7g	By Design	By Design	No
Fuselage_FrontLid	4h 21min	38.90g	%2 (Grid)	2	Yes
Fuselage_BackLid	2h 55min	18.38g	%2 (Grid)	2	Yes
Tilt_Mounts	1h 41min	11.37g	%15 (Grid)	4	Yes
Back_Mounts	1h 57min	13.46g	%15 (Grid)	4	No

As seen in the *Table 3.2*, the vehicle consists of 29 printing parts. Some of these parts such as Arms, Ailerons, Tilt_Mounts and Back_Mounts are suitable to be printed on the same plate file and the others are printed separately to prevent stringing. A total of 1230g of filament is used for the printed parts. However, considering the failed parts and the trials for quality improvements, approximately 2kg of filament was used. The parts with a total active printing time of 173h 22min were produced as a result of a 3-week process in total.

As mentioned in the detailed design section, the main parts are designed with internal structure. The number of walls was also determined at the design stage and was implemented on the solid models. For such printed parts, infill and wall line count features are indicated as By Design in the *Table 3.2*. The other parts designed as solid, infill and wall line count features were specified considering their weight and strength. For parts expected to be light weight, quality results were obtained by applying 2-3% infill and 1-2 wall count. Parts whose weight is not important but which need to be resilient, i.e. Arms and Mounts, 15% infill and 3-4 wall line count were preferred. Although most parts are designed in such a way that they do not need a support structure, it was necessary to activate support structure for some parts. In addition, the print orientations of the particular parts are given in the *Appendix H*.

3.3. Steps of Assembly Processes

- Assembly of the Wing & Tilt Mechanism**

The tilt mechanism is made from a servo motor, a BLDC motor, the mount for the BLDC motor, a bearing and a place for the servo inside the wing arm. Firstly, the servo horn and the bearing are attached to the sides of the motor mount and the motor was mounted using 4 m3 10mm screws. Then, a nut and the servo motor are placed inside the arm. Afterwards, the motor mount is attached to the arm by screwing an m3 12mm screw from the bearing side to the nut inside the arm. Lastly, the servo horn's screw is tightened. The full assembly of the tilt mechanism is shown in *Figure 3.3*.

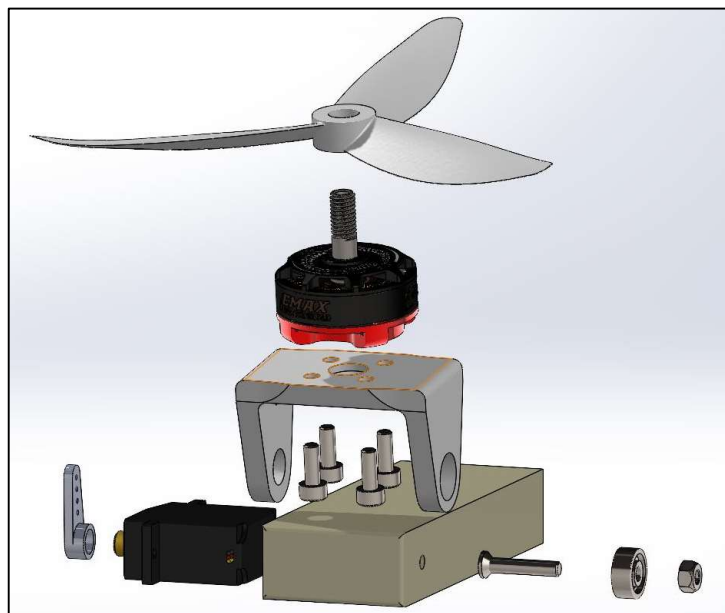


Figure 3.3 Exploded View of the Tilt Mechanism.

Due to the size of the wing and the available printer space, the wing is divided into 7 sections, 6 of which are shown in *Figure 3.4*, and the seventh one is the aforementioned wing arm. These sections of the wing are first aligned using pins and tabs made for alignment. These tabs and pins are added in order to ensure that the wing sections connect to each other accurately. The pin holes and tabs are shown in *Figure 3.5*.

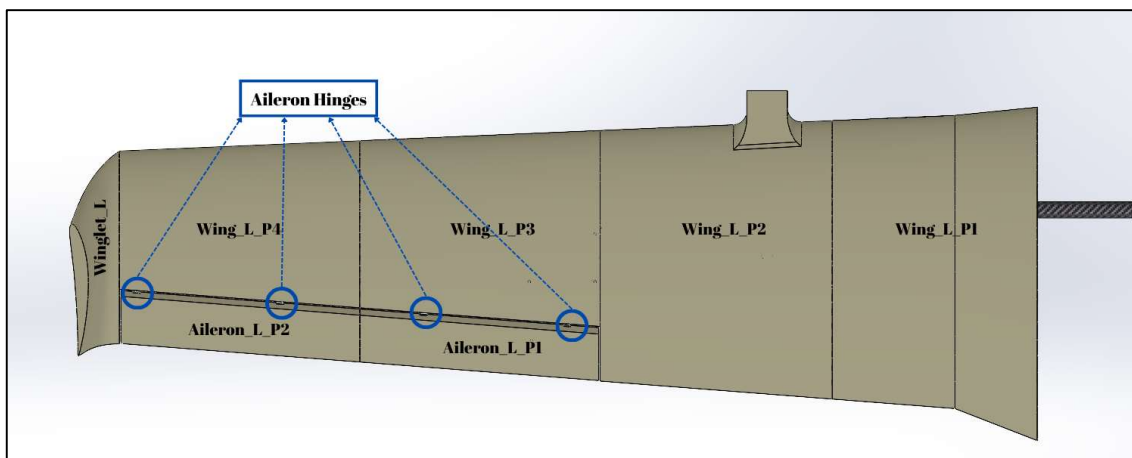


Figure 3.4 Divided Parts of the Wing.

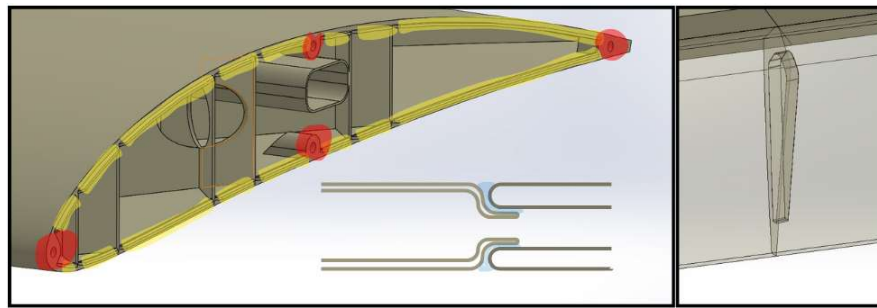


Figure 3.5 Tabs and Pin Holes Used on the Wing Sections.

The wing parts are connected using a cyanoacrylate glue with an activator, it can be seen in *Figure 3.6*. Cyanoacrylate glue is selected due to its strength, availability, low cost and fast curing. Also, the glue being two-part allows the necessary time needed for the alignment of the sections since the activator is only applied after the parts are in their correct place.



Figure 3.6 Gluing the Wing and Applying the Activator.

After the wing is glued together, the ailerons are attached using 3D printed hinges. Firstly, 1.2mm thick steel shafts was inserted for the hinges to rotate. Then hinges are glued to the aileron and the wing and connected as shown in *Figure 3.7*. Then the wing arm and the attached tilt mechanism is glued to the wing. Lastly, the fibre glass and epoxy composite spar pipes are inserted inside the wing as a tight fit. The fully assembled wing is also shown in *Figure 3.7*.

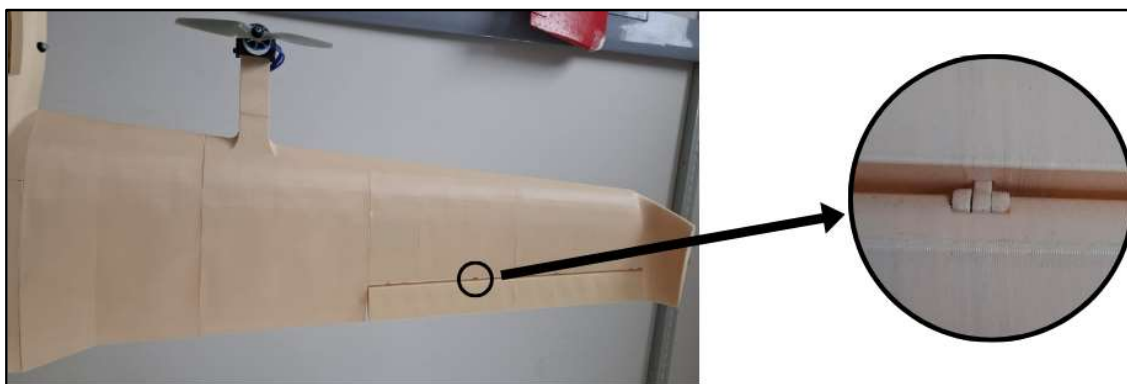


Figure 3.7 The Fully Assembled Wing and Hinge.

After the wing is assembled, the servos need to be attached to the wing in order to control the ailerons. To attach the servos, they are first screw on the inwards facing side of the servo caps that allow the servo horn to extend outside. Then, the servo is placed inside a cavity in the wing and it is covered by the servo cap which is screwed on the wing. This placement of the servos protects them from outside and creates a smoother surface. The servo cap is shown in *Figure 3.8*.

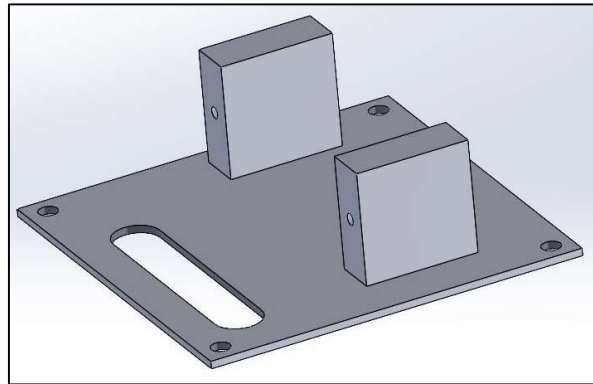


Figure 3.8 The CAD Model of Servo Cap used on the Wing.

- **Assembly of the Fuselage**

Similar to the wing, the fuselage is too large to be printed in one piece, therefore it is divided into 3 parts. Again, similar to the wing, the parts are first aligned using pins and holes, however no tabs are included in the connection of the fuselage parts. Then they are glued together using cyanoacrylate glue mentioned before. Afterwards, the tail pipe is connected to the back of the fuselage using a M3 screw and a nylon locknut. Lastly, another pipe is inserted through the fuselage, where the wings will be attached in order to stop the wing from rotating. The assembled fuselage is shown in *Figure 3.9*.



Figure 3.9 The Fully Assembled Fuselage.

In addition to the 3 parts, the fuselage also has 2 hatches. The back hatch allows access to the flight controller connections, electronic speed controller, buzzer, radio controller and wiring. The back hatch is attached to the fuselage using screws since these connections are not needed to be adjusted after the plane is completed, unless there is any issue.

The other hatch is placed towards the front of the plane. Through front hatch, it is possible to access the pitot tube and the battery. The battery needs to be removed and charged after flight; therefore, it needs to be accessed frequently. Therefore, the front hatch was attached using a spring latch mechanism. The mentioned hatches are given in *Figure 3.10*.



Figure 3.10 Front and Back Hatches on the Fuselage.

- **Assembly of the V-Tail**

The V-Tail is divided into 3 parts. There are the two stabilizers and one middle part to connect to the tail pipe. These parts are first aligned using pin holes, then glued together, similar to the wing assembly. No tabs are used since the connecting surface is also the printing surface, therefore it needs to be flat. The pin holes are shown in *Figure 3.11*.

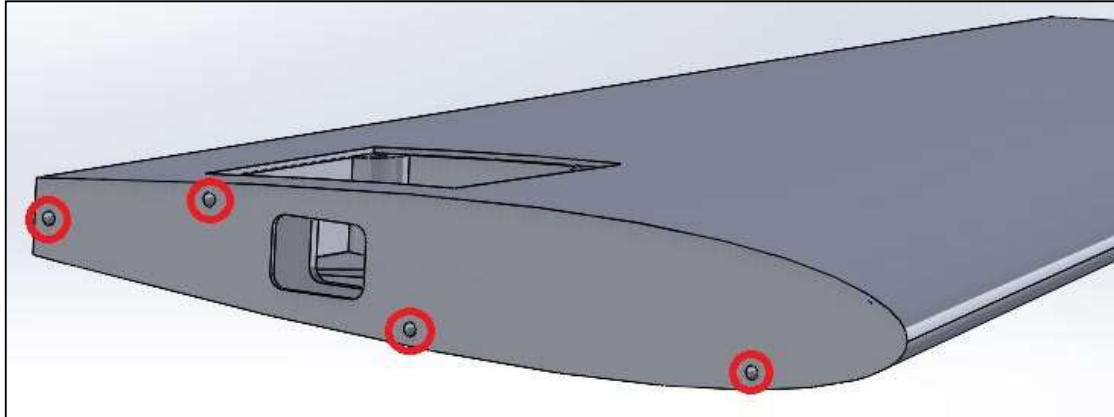


Figure 3.11 Pin Holes of the Tail.

Afterwards, the elevons are attached to the tail using the same 3D printed hinges used in attaching the ailerons to the wings. Lastly, the tail is attached to the tail pipe using a screw. This last connection mentioned is attached using a screw instead of glue in order to allow the tail to be removable. The assembled V-Tail is shown in *Figure 3.12*.

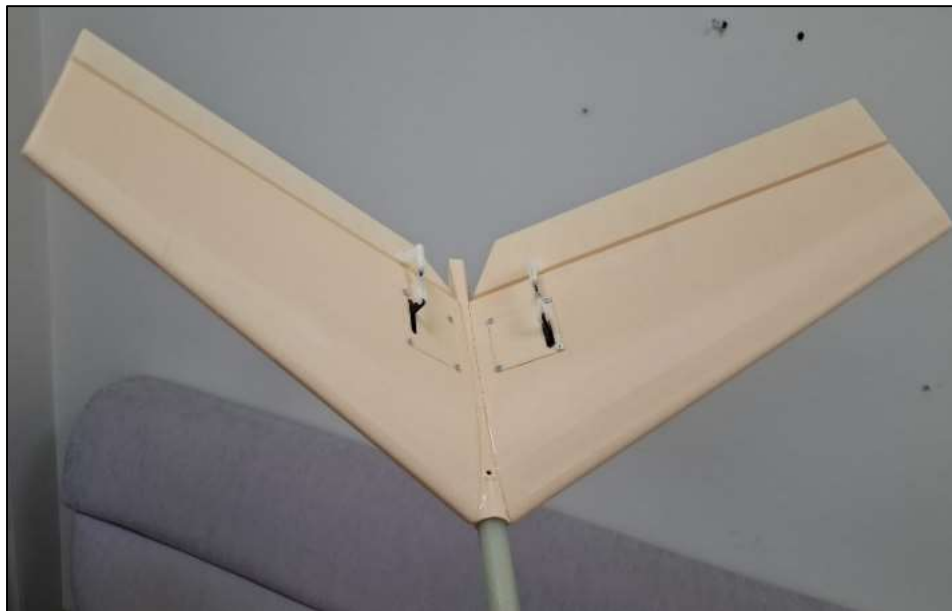


Figure 3.12 The Fully Assembled V-Tail.

After the tail is assembled, the servos that control the elevons are attached to the tail similar to the servos inside the wing. They are first screwed to the inward side of the servo cap, then they are placed inside the tail and the cap is screwed on.

During the first iteration of the assembly, it was observed that the middle part of the tail caved in during printing, which caused the entry for the tail pipe to be too small. Therefore, the design of this part was changed. The circular entry made for the tail pipe was converted into a tear drop shape.

• Electronic Wiring

After the mechanical assembly is completed, the next process to be carried out in the vehicle is the electronic wiring. The propulsion system generates the force that the vehicle will need during take-off and flight. The propulsion system of the vehicle consists of 3 Emax RS2205 BLDC motors equipped with 5045 3-blade propellers. Electronic Speed Controller (ESC), consisting of an array of mosfets and a microcontroller, is a device used to drive BLDC motors. GEPRC BLS60A 4in1 ESC, capable of conducting maximum of 60 Amper current to each motor, is selected for this purpose. Motor power is usually controlled by a PWM signal sent to the esc. However, in this system, the esc and therefore the motors are controlled by serial communication called DShot150. DShot communication is resistant to electrical noise and more accurate than PWM signalling. ESC signal wires are connected to AUX output of the controller.

The LiPo battery is connected to power module with 12 AWG cable and XT-60 connectors. The power module senses the current drawn and battery voltage and sends them to the controller as analogue signals. It also supplies 5V voltage the controller. Another 12 AWG cable connects output of the power module with power input of the ESC. Three 18 AWG wires coming from each motor is connected the motor outputs of the ESC with MR30 connectors.

Four MG90S Servo motors are attached to the vehicle to navigate the control surfaces. Besides that, two Emax ES09MD Servo motors are used to control tilt angle of the front motors. All of them are connected to Main output of the controller and driven by PWM signal. The controller is not equipped with hardware to power the servo rail. Power must be supplied from an external source. For this purpose, 5V BEC regulator which capable of supplying maximum of 3A current is also connected to servo rail. Input power to the regulator is delivered from the battery.



Figure 3.13 Pixhawk 2.4.8 Flight Controller.

The peripheral hardware is connected to the controller with Molex connectors and each of them drawn power directly from controller itself. As it can be seen in *Figure 3.13*, white pins are Molex ports. GPS is responsible to find global coordinates of the vehicle, and it delivers the data to the controller via UART communication. The air speed sensor is used to measure the relative wind speed flowing over the vehicle. The sensor, which makes the measurement using a pitot tube and a differential pressure sensor, transmits the data to the controller via I2C communication. Telemetry connected to the controller via UART, transmits the vehicle's states and parameters to the ground station. The telemetry also transmits the commands sent from the ground station to the controller, and packets and decodes the data with the MAVLink protocol.

In addition, the controller gives sound and visual notifications regardless of the ground station. These notifications indicate that the device is ready for flight, flight mode change, failsafe actions or reboot. While the buzzer provides audible interaction, the safety switch also provides visual notification with the LED on it. Furthermore, when the safety switch is activated, it kills the motors and provides precautions against accidents.

Table 3.3 Usage areas and Properties of Copper Wires according to American Wire Gauge (AWG).

AWG	Permissible Ampacity at 20°C (A)	Weight per Meter (gr/m)	Usage Field and Length
12	88	39	Main power line from battery to ESC (~0.4m)
18	22	11	Power line from ESC to motor (~2m)
24	5	4.5	Servo power and signal lines (~4m)
30	0.8	3.6	Peripherals power and signal lines (~0.5m)

All wiring in the vehicle is made using connectors and soldering technique. Cable thicknesses were decided according to AWG standards considering the maximum current passing through it. Important properties of the wires, fields of application and rough lengths of the cables are shown in the *Table 3.3*. A detailed schematic of the electronic wiring including avionics connections is provided in the *Appendix G*.

• Configuration of Autopilot

The final stage before the test flight is the configuration of the autopilot. The open source ArduPilot software allows control of various air, land and water vehicles. The software, which also supports various hardware models, offers hundreds of user-customised parameters for the selected vehicle type. With a large community support and detailed documentation, the software has been configured.

ArduPlane 4.6, the latest stable version of ArduPilot software developed for fixed wing and VTOL vehicles, has been installed. In the process, the Mission Planer software installed on the computer was used and fmuv3 setup compatible with the controller Pixhawk 2.4.8 hardware was preferred. Mission Planer program is a ground station software that is used to install the selected software on the controller, as well as for software configuration, parameter modification, live monitoring of flight data and semi-autonomous flight route planning. Mission Planer was used in the entire configuration process.

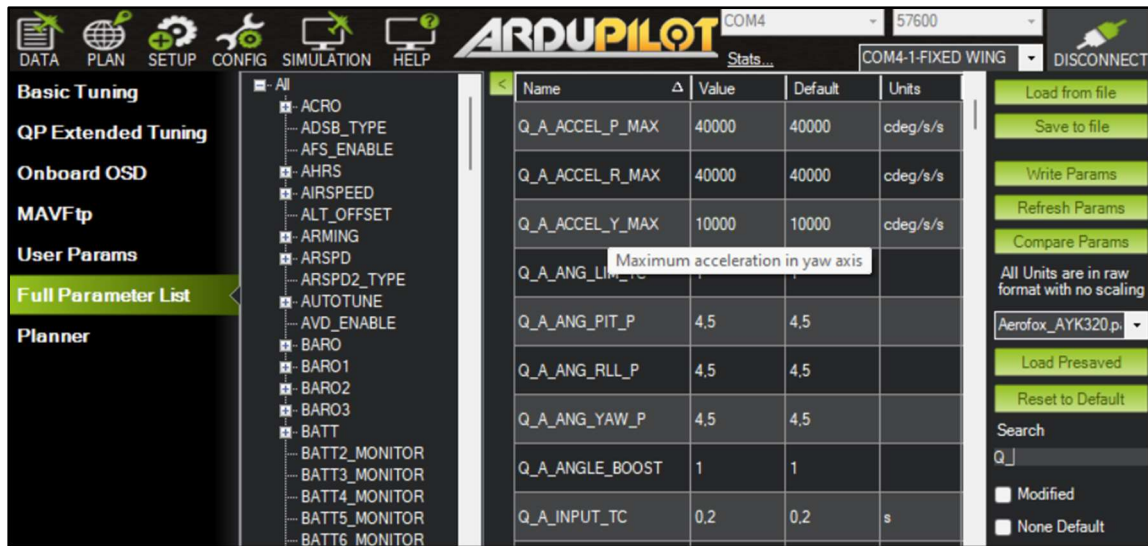


Figure 3.14 Mission Planer Full Parameter List Window.

For VTOL configuration, several parameters need to be changed. These parameters, their modified values and definitions are given in *Table 3.4*. In addition, after each parameter is changed, the parameter is written and the parameter list is refreshed. It can be done by clicking the green buttons on the right of the window in the *Figure 3.14*.

Table 3.4 Changed VTOL Configuration Parameters and their definitions.

Title of the Parameter	Default Value	Modified Value	Definition
Q_ENABLE	0	1	Indicates that the vehicle is VTOL and enables the VTOL parameters to be activated.
Q_TILT_ENABLE	0	1	Indicates that the VTOL vehicle has tilttable rotors.
Q_FRAME_CLASS	0	7	It allows to select a frame type, 7 indicates Tricopter layout and frame type.
Q_TILT_MASK	0	3	A bitmask that specifies which rotors can tilt, 3 stands for the front two motors.
Q_TILT_TYPE	0	2	it allows to choose the tilt modality. 2 means that its vectored, and tilt mechanism can control the yaw in vertical fight.
Q_TILT_RATE_UP	20	15	Selects the speed at which the motors will tilt upwards (degree/sec)
Q_ASSIST_SPEED	0	-1	For quad-in-plane vehicles, it specifies below which speed the vertical motors will assist lift. Deactivated.
Q_M_PWM_TYPE	0	5	Selects what type of signal the ESC will be fed with. 5 indicates DShot150 protocol.
Q_TRANSITION_MS	5000	7000	Determines how many milliseconds the transition process takes.
Q_M_BAT_VOLT_MAX	12.6	16.8	Indicates maximum battery voltage. 4S battery is 16.8 volts.
Q_M_BAT_VOLT_MIN	11.1	14.0	Indicates minimum battery voltage. Warning below set value.

Each channel in the servo rail of the controller must be assigned a function. The designed VTOL has 6 servos, two ailerons, two tail and two tilt mechanisms. They are connected to the MAIN output which has 8 ports, and the functions shown in the *Figure 3.16* are defined. 3 motors are connected to the aux output of the controller following the motor numbering shown in the *Figure 3.15*. The reason for this is that Pixhawk 2.4.8 can only generate the DShot signal at the AUX outputs. The first 8 numbers correspond to the first 8 MAIN outputs, while the 6 AUX outputs are numbered from 9 to 14 respectively.

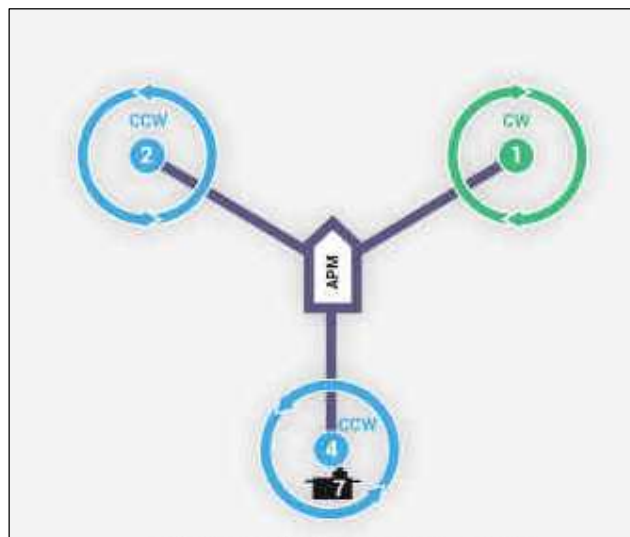


Figure 3.15 Ardupilot Tricopter Standard Motor Enumeration. [22]

#	Position	Reverse	Function	Min	Trim	Max
1	1450	<input type="checkbox"/>	VTailRight	950	1450	1950
2	1620	<input checked="" type="checkbox"/>	VTailLeft	1120	1620	2120
3	1500	<input checked="" type="checkbox"/>	Aileron	1100	1500	1900
4	1470	<input checked="" type="checkbox"/>	Aileron	1070	1470	1870
5	2200	<input type="checkbox"/>	TiltMotorFrontLeft	1100	1600	2200
6	900	<input checked="" type="checkbox"/>	TiltMotorFrontRight	900	1600	2000
7	1500	<input type="checkbox"/>	Motor7/TailTiltServo	1100	1500	1900
8	0	<input type="checkbox"/>	Disabled	1100	1500	1900
9	0	<input type="checkbox"/>	Motor1	1000	1000	2000
10	0	<input type="checkbox"/>	Motor2	1000	1000	2000
11	0	<input type="checkbox"/>	Disabled	1100	1500	1900
12	0	<input type="checkbox"/>	Motor4	1000	1000	2000

Figure 3.16 Mission Planer Servo Output Window

The connected servos that do not have the correct rotation direction are reversed by selecting the reverse option. The min and max values were set to 500 us in both directions for tail and 400 us in both directions for aileron. In the tilt mechanism, the angle at which the motors look straight ahead is given as max or min. The difference of 1100 us in the opposite direction is also given as either min or max.

3.4. Cost Analysis

The cost calculation of the project is not straightforward due to several reasons. The first one is that most of the electronics parts can be reused for other applications. Additionally, some of them has already in our stock. Therefore, it is proper to classify as the overall cost including every part and the budget that is specifically allocated for the project.

Table 3.5 The Overall Cost including every part.

Item	Pieces	Cost (₺)	Total Cost (₺)
PLA Filament	3	₺599.00	₺1.797.00
Adhesive & Equipment	1	₺500.00	₺500.00
Wing Spar Pipe	1	₺322.94	₺322.94
Tail Pipe	1	₺337.62	₺337.62
BLDC Motor	3	₺1056.00	₺3168.00
ESC	3	₺524.16	₺1572.48
Radio Controller	1	₺7340.00	₺7340.00
Tilt Mechanism Servo	2	₺643.97	₺1287.94
Control Surf. Servo	5	₺106.50	₺532.50
Pitot Tube	1	₺2140.00	₺2140.00
Propeller	3	₺54.42	₺163.26
Flight Controller	1	₺6770.00	₺6770.00
Battery	1	₺4257.00	₺4257.00
Total Cost:			₺30,000.74

As shown in *Table 3.5*, the overall cost includes every part. The total cost of the project is 30,188.74 ₦. Most of the cost are due to radio controller, flight controller and battery. Considering the complexity of the electronics used in aerial systems and the import costs, such prices are not surprising. However, the radio controller and flight controller are reusable, and the battery is borrowed. Therefore, the total cost decreases significantly, when the reusable and borrowed parts are excluded. As shown in *Table 3-6*, the total cost falls to 3,120.82 ₦.

Table 3.6 The cost that is specifically allocated for the project

Item	Pieces	Cost (₦)	Total Cost (₦)	Usability
PLA Filament	3	₦599.00	₦1,797.00	-
Adhesive & Equipment	1	₦500.00	₦500.00	-
Wing Spar Pipe	1	₦322.94	₦322.94	-
Tail Pipe	1	₦337.62	₦337.62	-
BLDC Motor	3	₦0.00	₦0.00	Reusable
ESC	3	₦0.00	₦0.00	Reusable
Radio Controller	1	₦0.00	₦0.00	Reusable
Tilt Mechanism Servo	2	₦0.00	₦0.00	Reusable
Control Surf. Servo	5	₦0.00	₦0.00	Reusable
Pitot Tube	1	₦0.00	₦0.00	Reusable
Propeller	3	₦54.42	₦163.26	-
Flight Controller	1	₦0.00	₦0.00	Reusable
Battery	1	₦0.00	₦0.00	Borrowed
Total Cost:			₦3,120.82	

At the end of the chapter, it should not be forgotten that it is an estimated and rough calculation made in today's conditions. Prices may change at the end of the year due to factors such as inflation, tax rates and stock-outs.

4. Project Management

The path needs to be followed in the design of a VTOL aircraft is not straightforward. At some stages, retrospective updates would be required to achieve better results. For example, at the angle of attack where the wing generates sufficient lift could not be the angle where the vehicle is at static equilibrium. In such case, it may appropriate to find retrospective solution such as redesigning the wing or changing the airfoil. Through the research, such design phases were learnt before starting the project and a design pathway was established. The progress tree showing the design steps is shown in *Figure 4.1*.

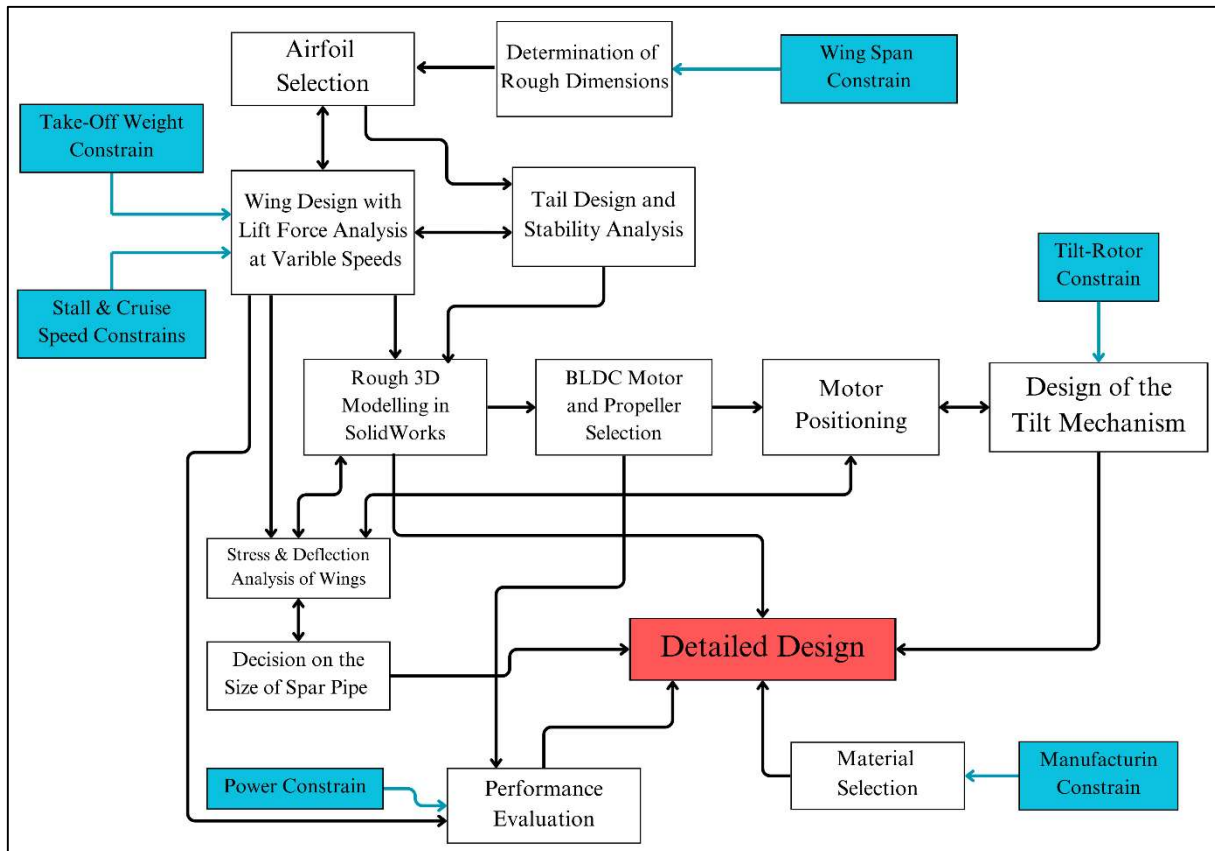


Figure 4.1 The Progress Tree of VTOL Design Process.

In *Figure 4.1*, blue coloured boxes indicate design constrains mentioned in introduction. Also, retrospectively dependent stages are connected by bidirectional arrows drawn between each other. Detailed design develops by combining semi-dependent stages. Each completed stages finds its places in the detailed design. The design phases shown in *Figure 4.1* were used to create a Gantt Chard.

Most stages of the design process were carried out as a team. Although the works done individually are generally not suitable to be done as a team; ideas and important points were discussed before and after the work. In case of that the member encounters a problem during the work, possible solutions and approaches have been investigated and decided as a team. The analyses and designs using XFLR5 were done as a team since we both wanted to learn the program individually. Metin has carried out 3D modelling of the wing and fuselage, numerical deflection analysis and finite element analysis. Harun has carried out 3D modelling of the tail, designing and modelling of tilt mechanism and the servo actuator selection. BLDC motor selection, Material selection and performance evaluation have been carried out together.

During the manufacturing process, some tasks were divided between individuals and some tasks were done as a team similar to the design process. Metin carried out the 3D printing of the fuselage, wings and ailerons, done the wiring of the electronics and configured the software to be suitable for the manufactured VTOL. Harun carried out the 3D printing of the tail, elevons and the parts for the tilt mechanism and assembled the tilt mechanism. Ömer carried out the assembly of the wing and the fuselage, and was responsible for the stability analysis of the assembled vehicle using the measured inertias of the assembled vehicle. The market research for the required materials, the full assembly of the aircraft and the test flights were performed as a team.

Gantt Chard is a table contains activities that need to be done in order to complete a project. It also contains the time these activities are expected to take. Even though all stages were started on time, some stages could not be completed in expected time. The reason behind this can be poor prediction of required time for subtask or seasonal labour intensity. Stages not completed on time are Airfoil Selection, Motor & Propeller Selection and Tilt Mechanism Design tasks as it can be seen in *Figure 4.2*.

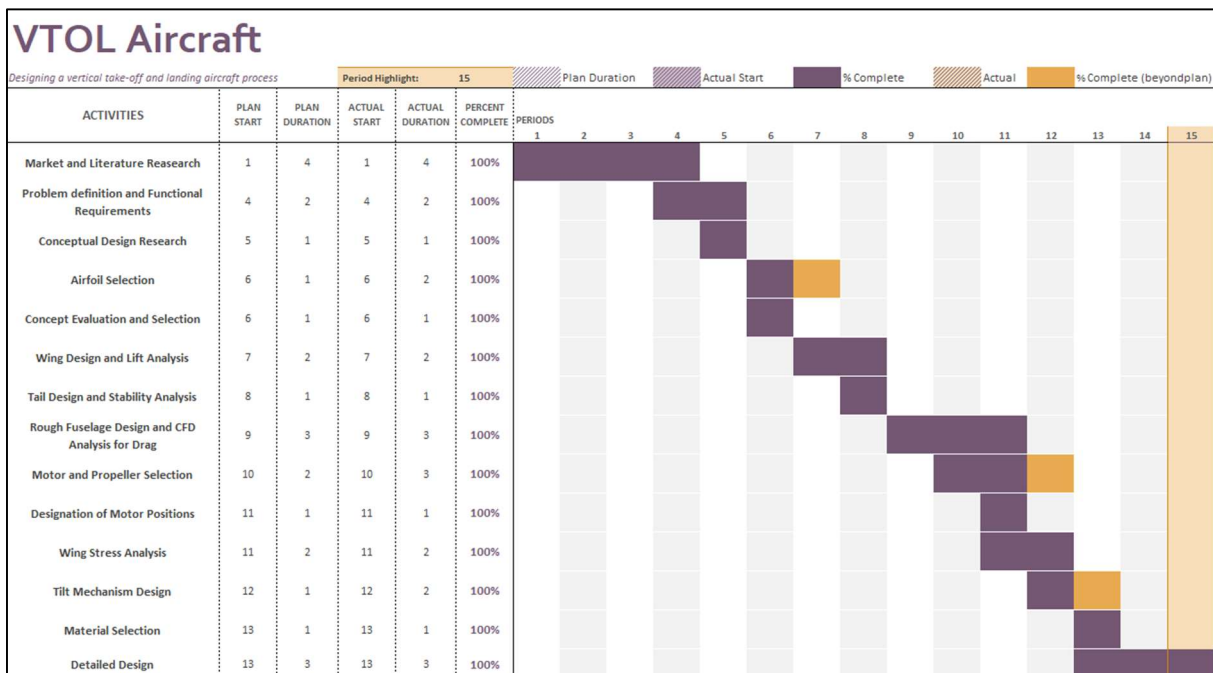


Figure 4.2 The Gantt Chard of the Designing of the VTOL aircraft for ME429.

Another Gantt chard for the next step which was carried out in ME492 course of the project is also provided in *Figure 4.3*. The designed aircraft was manufactured in this semester. The stages of the production process and time each of them took are listed. Due to unforeseen problems that occurred during the semester, some tasks were delayed. This caused other tasks that rely on the previous tasks to also be delayed. Also, the finalization of the fuselage design and its manufacture was moved to a later date; however, they were carried out in parallel to other tasks so this did not cause much total delay.

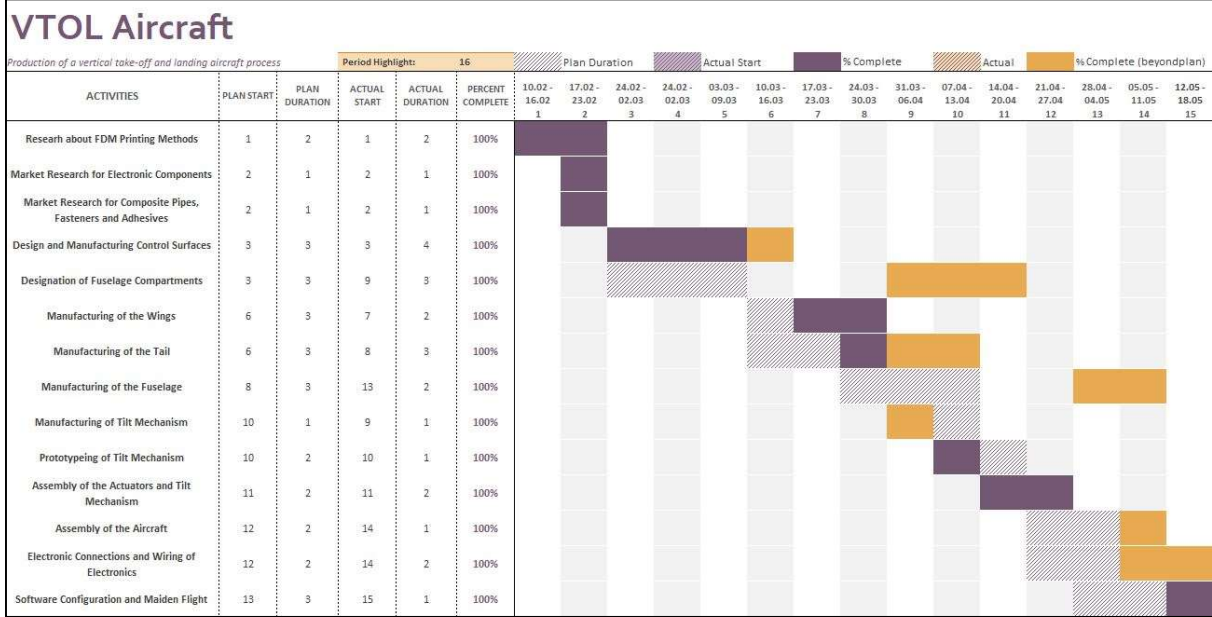


Figure 4.3 The Gantt Chard of the Production of the VTOL aircraft for ME492.

5. Discussion

XFLR5 was the tool that helped us most in the finalisation of the design process. As mentioned in detailed design and analysis section, it was benefited in many fields. There were other options to be used in design section such as XFOIL. It was developed Mark Drela from MIT [30]. XFOIL is capable of viscid/inviscid analysis of existing foils, it can generate multiple polars like XFLR5 and give pressure distribution of the airfoil. Generally, XFOIL is used with Matlab to generate polars. In this way, entire wing can be modelled numerically, and also dynamic stability of the system can be examined using Aerospace Toolbox of Simulink. However, it could be time-consuming process. Even though such way gives a better understanding of the underlying mechanics by building everything from scratch, it was decided that it was more important to use time in efficient way. On the other hand, XFLR5 provides the user with plenty of parameters to modify as needed. As can be seen in the *Figure 5.1*, XFLR5 also has an interface supported by 3D graphics where it can display the results of the analysis. The visual representations are not obtained as a result of Finite Element Computational Fluid Dynamics analysis. There have been added to the program to give and visual idea. Therefore, it is not mentioned in the analysis section.

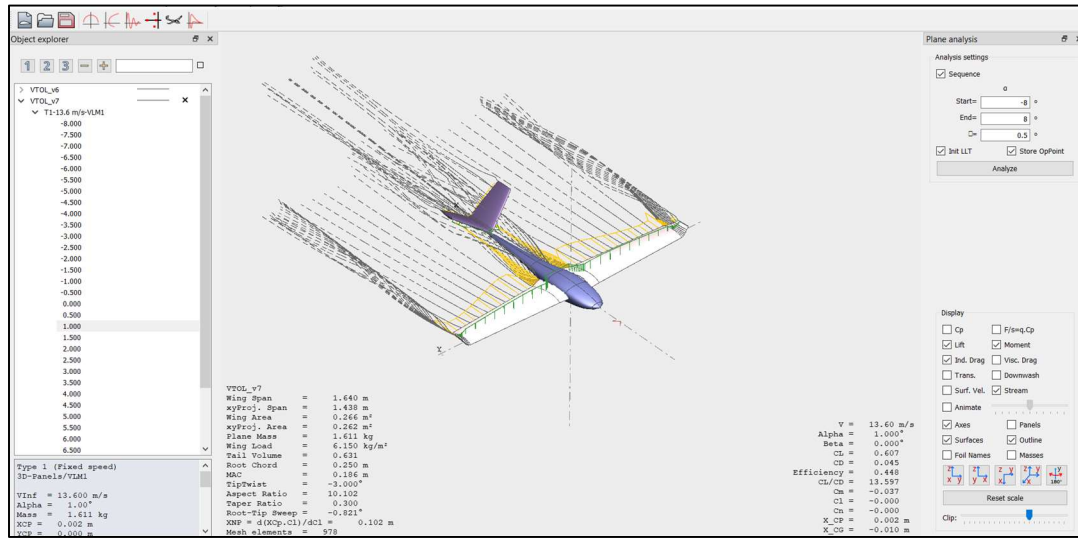


Figure 5.1 An Example of XFLR5 User Interface.

At the end of the structural analysis of the wing, it was aimed to perform Finite Element CFD Analysis for the vehicle. It was planned to obtain the total drag force that the vehicle experienced at cruise speed, and also examines airflow separation at high angle of attacks. Analyses attempted using Ansys Fluent did not give reasonable results. The reason behind this was investigated and it was found that creating a sufficiently fine mesh is important for convergent results. When a finer mesh was tried to be generated, problems were encountered due to the insufficient processing power of the computers used.

A different mesh problem was also encountered in structural analysis. In finite element analysis, the mesh quality has a direct influence on the result. Due to the complexity of the geometry, some meshing methods have failed. These failures were appeared as non-formed mesh in some cases or due to poor mesh quality. By using Hex method with sizing of *1mm*, it was achieved an acceptable mesh. “Mesh Metrics” tool provided in Ansys was used to check the quality of the mesh. It allows the quality of the mesh to be evaluated using different methods. Element quality method shows how convergent the element is to the ideal cube. 1 indicates a perfect cube, while 0 stands for an element without volume. The quality results of the meshes used in the analysis is shown in the *Figure 5.2*. As can be seen, there is no faulty element and more than 70% of the elements have a quality above 0.9.

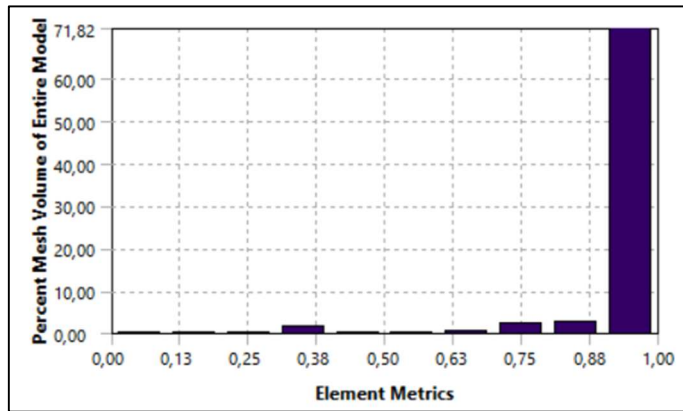


Figure 5.2 The Element Quality Result of the Structural Analysis.

Another quality examination method of meshing is the Jacobian ratio method. The Jacobian ratio is used to express the similarity of an element to the shape of the ideal element. The ratio of an ideal element is 1 as expected. The Jacobian ratio of a good quality mesh element is expected to be in the range of 1 to 10. Observing the *Figure 5.3*, it can be seen that almost 80% percent of the elements fall within the range.

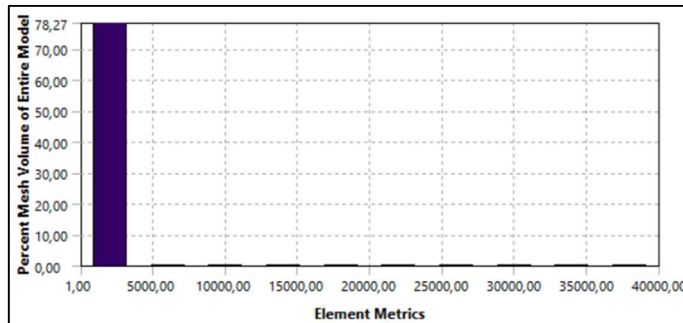


Figure 5.3 The Jacobian Ratio Result of the Structural Analysis.

The whole structural analysis process was conducted based on FDM printed PLA material. However, it is also considered to use LW-PLA in the tail and wing members to reduce the take-off weight. The material, which can be printed in different densities according to the printing temperature, is considered to be used in places such as winglets and tails subjected to low stresses. With this method, a weight reduction of 80 g in the tail and 20 g each in the winglet can be achieved. The reason why PLA is chosen in other printed components is that there is no detailed study on the mechanical properties of LW-PLA. If research on LW-PLA materials printed at different temperature settings had been conducted, it could prove to be a more suitable material than PLA for such application.

When the design phase was completed, it was planned to finish the vehicle with a final weight of 1950gr. Excepted value was exceeded due to the use of glass pipes instead of carbon pipes, the use of adhesives and weight of the wires. The final weight of the vehicle is 2340gr. Thanks to the safety factor application in the static analysis process, the structure of the vehicle still remained in the safe margin.

Examples of this efficiency-targeted combination of different types of aircraft are currently rare. However, works are being conducted on similar VTOL designs, especially in the field of cargo transportation. It is quite likely to become a part of our regular life in the near future. The experiences we have gained through the final project may make us preferable engineers in that field. Even if this is not the case, undertaking such a comprehensive design report has taught us how to use the knowledge we have gained throughout our education.

6. Conclusion

The technological innovations have been allowing more flexibility over designs of air vehicles, as new manufacturing techniques like additive manufacturing have emerged. Additionally, there is increasing availability of electronics and open-source software. This flexibility is clearly reflected in the new concepts in unmanned air vehicles. As this project showed, VTOL UAVs are one of these concepts. Among VTOL aircrafts, tiltrotor air vehicles have been getting a lot of attention. This largely results from their scalability, application of precision, and desirable hover efficiency.

In the design process, design criteria are chosen according to Product Design Specification. This method is a very comprehensive process that includes vital prerequisites and limitations and features. In this process, eleven features are chosen. These features classified into three categories as performance requirements, operation requirements, and manufacturing requirements. By using Binary dominance, their importance are hierarchically organized with their weighting. It is found that control stability is the most important parameter with 0.167 weight. Then, possible concepts in tiltrotor VTOLs are explored. These concepts are three-rotor, four-rotor, and two-rotor VTOLs. Then, these concepts are compared with the weightings acquired in the dominance matrix. It is concluded that three-rotor tiltrotor VTOL aircraft has the highest grade with the grade difference of 0.58 over 6 to its closest concept.

In the next step, the research on airfoils is done. Three types of NACA airfoils are selected as NACA-6412, NACA-4412, and NACA-2412. The values of lift coefficient and drag coefficient for given Reynold numbers and angle of attack of these airfoils meets the desired expectations. In the next phase, the design of wing is carried out. In this process, minimum of 15 N lift at speed of 13m/s is required. By using XFLR5 software, the wing is designed in multiple iterations, by changing either airfoil profile or wing shape. In the final design, 1.640 m wingspan and NACA-6412 airfoil profile is decided for optimal lift at stall and cruise speed. In the next stage, tail design is carried out, using XFLR5 software. In the design, the calculations of moments of both wing and tail are carried out. Then, the design of tail is finalised, after the static stability is taken into account.

Detailed 3D design of parts and dynamic stability analysis are carried out. XFLR5 does not provide internal structure for the parts. Therefore, the parts are designed in SolidWorks, according to the stresses they exposed. For the stress analysis, composite tube and the shell of the wing is considered for simplification. Then according to the results, internal grids are added to the structure. Afterwards, the moment of inertias of wing and tail derived in SolidWorks is uploaded to the XFLR5 for dynamic stability. Additionally, electronics and other significant masses are manually added as point masses to XFLR5. Dynamic analysis can be classified into two main modes, as longitudinal modes and lateral modes. With the tools provided by XFLR5, these modes are analysed. It is concluded that the plane can stabilise itself less than a second in Short-Period mode, while settling time of Phugoid mode is nearly 1.5 minutes. In lateral modes, the Spiral Mode is unstable for the plane. However, this can be easily handled by the flight controller. The other types in lateral modes performs sufficiently for the plane.

For a reliable vertical flight, the thrust for each rotor is calculated. Then, the market research is carried out for proper rotors. Emax RS2205S-2300Kv model BLDC motors with 3 blade 5045 propeller is chosen for each rotor. After that, Emax ES09MD Dual-Bearing servo actuators for tilting mechanism is chosen. In the next step, the designation of rotors is done as the rotors are selected. The positioning of the rotors is done according to wing position and the proper force balance of rotors. After that step, tilting mechanism is designed. The direct connection between servo motor and the rotor is preferred, because of its simplicity and stable structure. The design of tilting mechanism is integrated to the wing. Then the mounting unit is designed for the back rotor.

As the design of the tilting mechanism is finalised. The structural analysis of the wing is applied with Ansys. The mechanical properties of PLA which is expected to be used in the manufacturing is derived from experimental results. In this analysis, the spar tubes are integrated to the analysis for more accurate results. The results from the analysis have given additional confidence for the structural strength of the design.

In the next part, the performance of the aircraft is evaluated. The main consideration in its evaluation is power consumption. Power consumption is calculated for horizontal and vertical flight with transition phase. With the chosen battery, the aircraft has a flight time up to 8.5 with a range 5.9 km. In the next part, cost analysis is done in two categories as mechanical parts and electronic parts. From the analysis, total expenditure is expected to be 30,000.74€ which most of the cost comes from electronics. Finally, management of the project is explained. The planning is laid out in the progress tree, as it shows the interconnections with each part. As the flow on the design process showed, planning is not straightforward. There were some minor changes in the planning. While some of the work is done collectively, the rest is carried out individually by the project members.

For the manufacturing, selection of material and manufacturing process are very closely related, since the additive manufacturing is chosen as a method. Consequently, Filaments are chosen as a manufacturing material. Among the filaments, PLA and ABS were very good option for the project. PLA offers very good mechanical properties for most of the parts in the plane, while ABS are used in critical areas due to its high softening temperature and high impact strength. Then the GFRP tubes are used to support wings internally and as a connection unit. In the manufacturing Creality's Ender3-S1 printer is chosen, because of availability. It is used with mainly Prusa Slicer which offered very good slicing.

In the assembly process, the wings, the fuselage, and the tail are divided to fit the 3D printer. Afterwards, they are assembled part by part. Eventually, the whole frame is assembled. In the next part, the electronic wiring is carried out including all the electronics. After the electronic wiring is done, the autopilot is configured on the controller. ArduPilot is chosen as open-source software, thanks to its community support and detailed documentation.

In discussion part, XFOIL feature of XFLR5 software is explained to give a better understanding of the software. Additionally, the use of this feature is explained with given reasons. Then, Finite Element CFD analysis is performed in Ansys. However, the desired results were not obtained due to complexity of the meshing and lack of understanding on this topic. Additionally, the use of LW-PLA in the manufacturing is discussed, since it has significantly lower density than conventional PLA filaments.

References

- [1] “How Additive Manufacturing is Accelerating Drone Production,” AMFG, 31 May 2024. [Online]. Available: <https://amfg.ai/2024/05/31/how-additive-manufacturing-is-accelerating-drone-production>.
- [2] A. Avitan, “The Differences Between UAV, UAS, and Autonomous Drones,” Percepto, 03 Jan 2019. [Online]. Available: <https://percepto.co/what-are-the-differences-between-uav-uas-and-autonomous-drones/>.
- [3] “Iris - The Ready to Fly Quadcopter,” APM Copter, 19 Aug 2013. [Online]. Available: <https://www.arducopter.co.uk/iris-quadcopter-uav.html>.
- [4] Z. Blackwood and G. . S. King, “Vertical Take-off Unmanned Aerial Vehicle with Forward Flight Transition,” *The West Indian Journal of Engineering*, vol. 40, no. 2, pp. 62-71, 2018.
- [5] E. Gökböl, A. Güllü and S. Ersoy, “Improvement of UAV: design and implementation on launchability,” *Aircraft Engineering and Aerospace Technolog*, vol. 95, no. 5, pp. 734-740, 2023.
- [6] P. Degond, A. Diez and M. Na, “Bulk topological states in a new collective dynamics model,” Department of Mathematics, Imperial College London, London, United Kingdom, 2021.
- [7] B. W. Everstine, “Lockheed Looking at Extending the F-35’s Range, Weapons Suite,” 17 Jun 2019. [Online]. Available: <https://www.airandspaceforces.com/lockheed-looking-at-extending-the-f-35s-range-weapons-suite/>.
- [8] “Facts and Figures About the F35 Fighter Jets,” Guernsey Press, 18 Aug 2018. [Online]. Available: <https://guernseypress.com/news/uk-news/2018/08/18/facts-and-figures-about-the-f-35-fighter-jets/>.
- [9] “V-22 Osprey,” Boeing, [Online]. Available: <https://www.boeing.com/defense/v-22-osprey>.
- [10] “VTOLs Guide,” PX4, [Online]. Available: https://docs.px4.io/main/en/frames_vtol/.
- [11] “Controller Diagram,” PX4, [Online]. Available: https://docs.px4.io/main/en/flight_stack/controller_diagrams.html.
- [12] C. Pan, J. Zhang , D. Zhang and L. Yu, “Modeling and Attitude Control of a Tilt Tri-Rotor UAV,” in *Proceedings of the 36th Chinese Control Conference*, Dalian, China, 2017.
- [13] H. Bang and J. Liao, “Transition Nonlinear Blended Aerodynamic Modeling and Anti-Harmonic Disturbance Robust Control of Fixed-Wing Tiltrotor UAV,” *Drones*, vol. 7, no. 225, 2023.

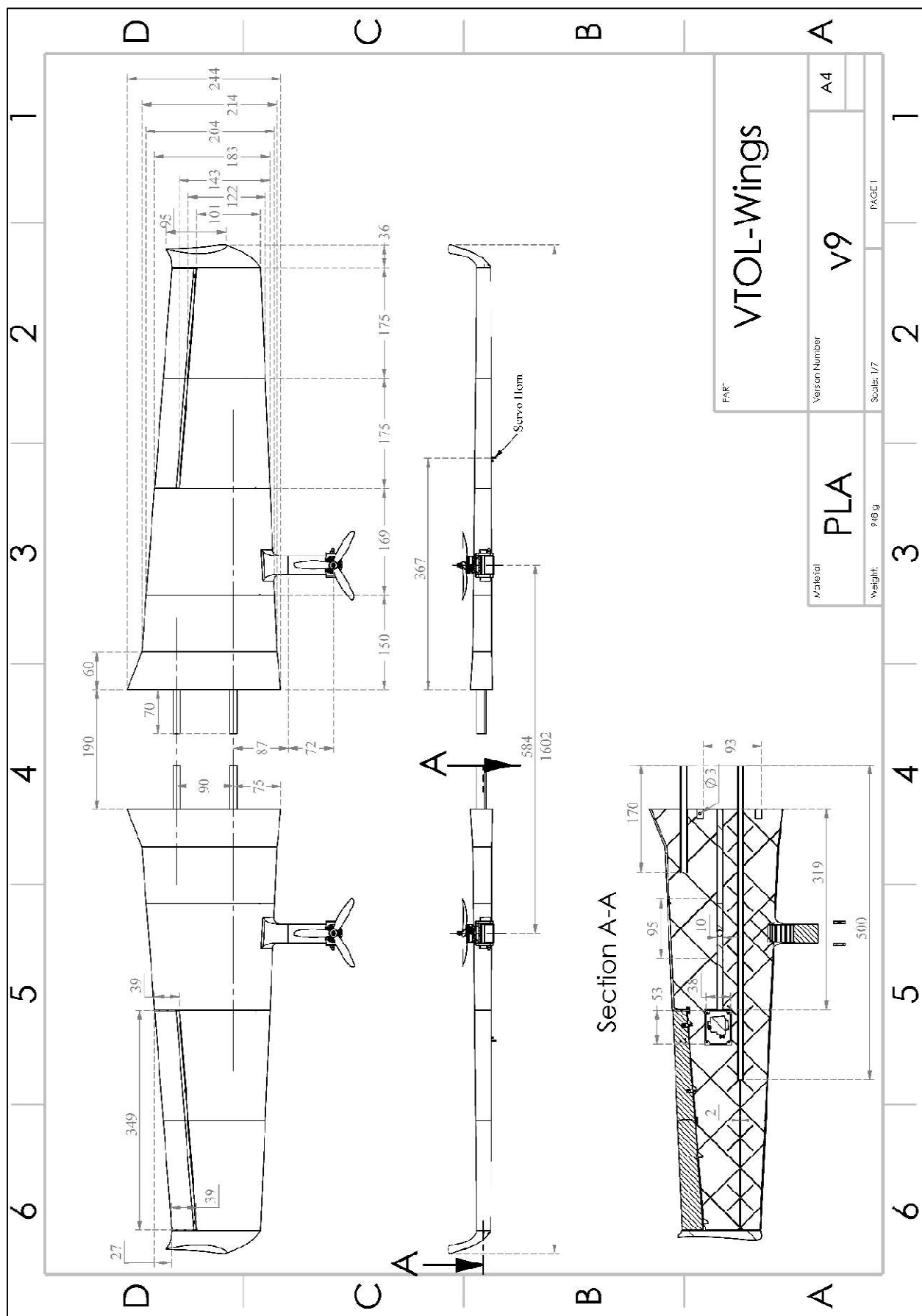
- [14] S. Krishna, Y. Siva and S. Panigrahi, “Design, Analysis, and Testing of a Hybrid VTOL Tilt-RotorUAV for Increased Endurance,” *Sensors*, vol. 21, no. 5987, 2021.
- National Aeronautics and Space Agency, “NASA History,” 2023 May. 11. [Online].
[15] Available: <https://www.nasa.gov/reference/the-national-advisory-committee-for-aeronautics/>.
- E. N. Jacobs, K. E. Ward and R. M. Pinkerton, “The characteristics of 78 related airfoil [16] sections from tests in the variable-density wind tunnel,” National Advisory Committee for Aeronautics, Washington, D.C., 1933.
- A. Marta and P. Gamboa, “Long Endurance Electric UAV for Civilian Surveillance [17] Missions,” in *29th Congress of the International Council of the Aeronautical Sciences*, St. Petersburg, Russia, 2014.
- D. Scholz, “Empennage Sizing with the Tail Volume,” *INCAS BULLETIN*, vol. 13, no. 3, [18] pp. 149-164, 2021.
- A. C. UGURAL and S. K. FENSTER, “5.9 Composite Beams,” in *Advanced Mechanics of [19] Materials and Applied Elasticity (Sixth Edition)*, Pearson, 2020, pp. 270-273.
- R. C. Hibbeler, “12.2 Slope and Displacement by Integration,” in *Mechanics of Materials*, [20] Pearson, 2018, p. 599.
- H. Smith, “Dynamic Stability,” in *Aircraft Flight Mechanics*, 2022.
- “ArduPilot,” [Online]. Available: <https://ardupilot.org/ardupilot/>.
- T. Yao, J. Ye, Z. Deng, K. Zhang, Y. Ma and H. Ouyang, “Tensile Failure Strength and [23] Separation Angle of FDM 3D printing PLA Material,” *Composites Part B: Engineering*, vol. 118, 2020.
- G. Staples, “Propeller Static & Dynamic Thrust Calculation,” 12 April 2014. [Online].
[24] Available: <https://www.electricrcaircraftguy.com/2014/04/propeller-static-dynamic-thrust-equation-background.html>.
- “What is a 3D Printer Filament: Definition, Types and Uses,” [Online]. Available: [25] <https://www.raise3d.com/academy/what-is-3d-printer-filament/>. [Accessed 9 June 2025].
- “Polylactic Acid (PLA) 3D Printing Filament Review,” [Online]. Available: [26] <https://juggerbot3d.com/pla-filament-review/>.
- “Acrylonitrile Butadiene Styrene (ABS) 3D Printing Filament Review,” [Online]. Available: [27] <https://juggerbot3d.com/3d-printing-material-capabilities/abs-filament-review/>.

- [28] Y. X. J. F. Meiyu Li, “Orthotropic mechanical properties of PLA materials fabricated by fused deposition modeling,” <https://doi.org/10.1016/j.tws.2024.111800>, vol. 199.
- [29] J. Qureshi, “A Review of Fibre Reinforced Polymer Structures,” <https://www.researchgate.net/>, 2022.
- [30] L. Clark, “Faculty profile: Mark Drela’s Researchs,” *AeroAstro Magazine*, 2006.

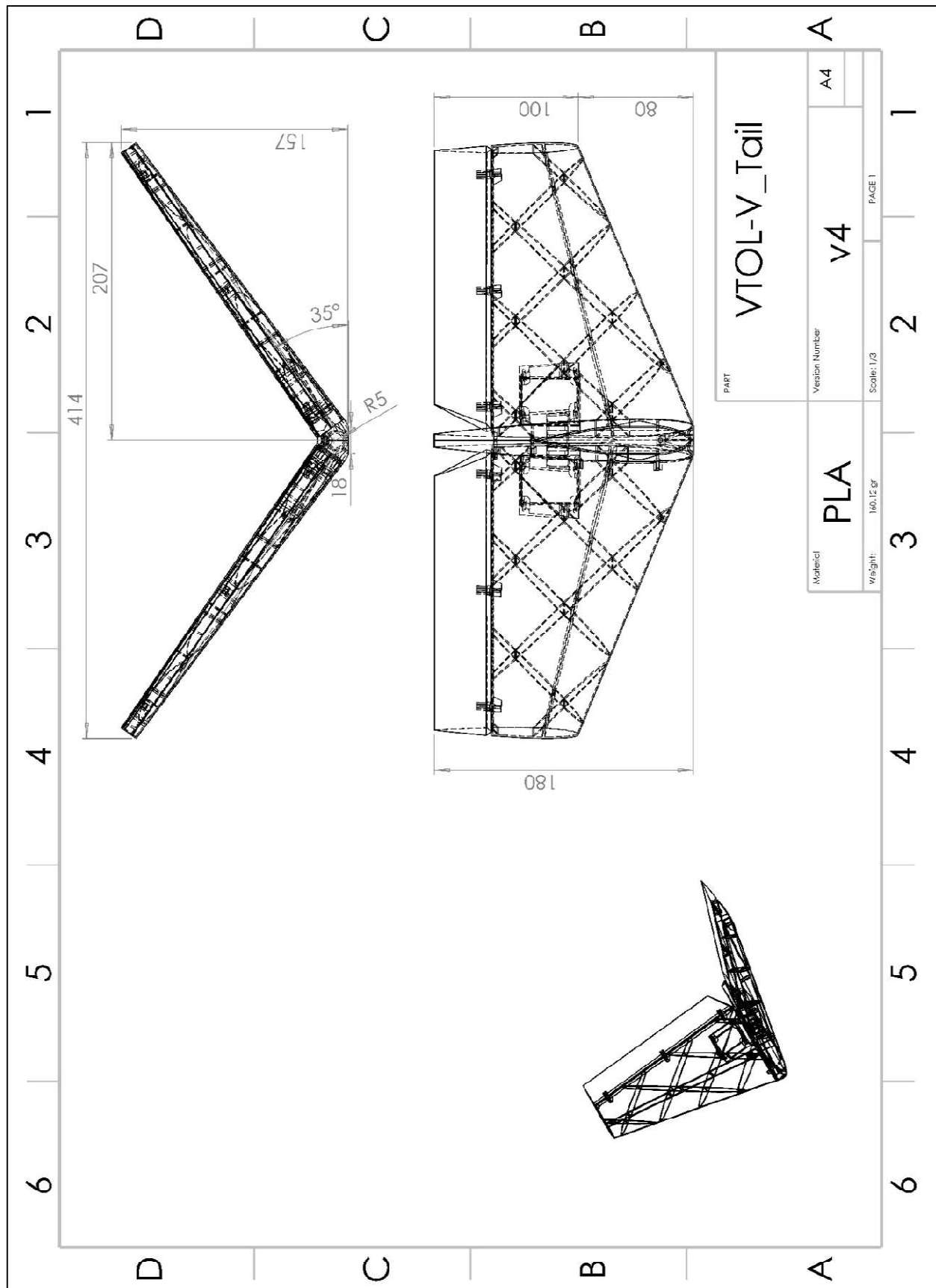
Appendices

<i>Appendix A: The Technical Drawings of the Wings.....</i>	55
<i>Appendix B: The Technical Drawing of the V-Tail.....</i>	56
<i>Appendix C: MATLAB Code for Numerical Deflection</i>	57
<i>Appendix D: The Technical Drawing of the VTOL Assembly.</i>	58
<i>Appendix E: Technical Drawing of the Tilting Mechanism.....</i>	59
<i>Appendix F: Technical Drawing of the Rear Motor Mount.....</i>	60
<i>Appendix G: The Wiring Diagram of the V-TOL</i>	61
<i>Appendix H: Print Orientations of Selected Parts.</i>	62

Appendix A: The Technical Drawings of the Wings



Appendix B: The Technical Drawing of the V-Tail



Appendix C: MATLAB Code for Numerical Deflection

```
% Imported data from xflr5
wing_y = [-0.815 -0.805 -0.7975 -0.7925 -0.7875 -0.7825 -0.7775 -0.7725 -0.7675 0.7625 -0.7588 -0.7562 -0.7538 -
0.7512 -0.7161 -0.6483 -0.5806 -0.5128 -0.445 -0.3772 -0.3094 -0.2417 -0.1739 -0.137 -0.131 -0.125 -0.119
-0.113 -0.107 -0.101 -0.095 -0.089 -0.083 0.089 0.095 0.101 0.107 0.113 0.119 0.125 0.131 0.137
0.1739 0.2417 0.3094 0.3772 0.445 0.5128 0.5806 0.6483 0.7161 0.7512 0.7538 0.7562 0.7588 0.7625 0.7675
0.7725 0.7775 0.7825 0.7875 0.7925 0.7975 0.805 0.815];
M_b_hrz = [0 0.0004 0.0013 0.002 0.003 0.0041 0.0055 0.0071 0.0088 0.0106 0.012 0.0128 0.0137 0.0146 0.0258 0.1201
0.3031 0.5857 0.976 1.48 2.1015 2.8414 3.6968 4.2199 4.3059 4.3927 4.4801 4.5682 4.6569 4.7462 4.836
4.9263 5.0169 5.0169 5.0169 4.9263 4.836 4.7462 4.6569 4.5682 4.4801 4.3927 4.3059 4.2199 3.6968 2.8415
2.1015 1.48 0.976 0.5857 0.3031 0.1201 0.0258 0.0146 0.0137 0.0128 0.012 0.0106 0.0088 0.0071 0.0055
0.0041 0.003 0.002 0.0013 0.0004 0];
chord = [0.08 0.09 0.0975 0.1025 0.1075 0.1125 0.1175 0.1225 0.1275 0.1325 0.1362 0.1387 0.1412 0.1437 0.1492
0.1575 0.1658 0.1742 0.1825 0.1908 0.1992 0.2075 0.2158 0.2215 0.2245 0.2275 0.2305 0.2335 0.2365 0.2395
0.2425 0.2455 0.2485 0.2485 0.2485 0.2455 0.2425 0.2395 0.2365 0.2335 0.2305 0.2275 0.2245 0.2215 0.2158
0.2075 0.1992 0.1908 0.1825 0.1742 0.1658 0.1575 0.1492 0.1437 0.1412 0.1387 0.1362 0.1325 0.1275 0.1225
0.1175 0.1125 0.1075 0.1025 0.0975 0.09 0.08];
% Vertical Flight Bending Moment
M_b_vrt = 9.81*2*(0.815-abs(wing_y));
d_o = 0.012; % Outer diameter of the tube [m]
d_i = 0.010; % Inner diameter of the tube [m]
A_tube = pi * (d_o^2 - d_i^2) / 4; % Tube Area [m^2]
I_tube = pi * (d_o^4 - d_i^4) / 64; % Tube moment of inertia [m^4]
E_tube = 39e9; % Elastic modulus of CFRP [Pa]
d_st = (1.22e-2) * chord; % Distance btw General Neutral Axis and Tube Neutral Axis [m]
I_tube_transformed = I_tube + A_tube*d_st.^2; % Transformed I of shell
L_tube = 0.5; % Length of the tube in half of the wing [m]
I_shell = (55082.565563e-12/0.25^3) * chord.^3; % Shell moment of inertia [m^4]
E_shell = 1.951e9; % Elastic modulus of PLA [Pa]

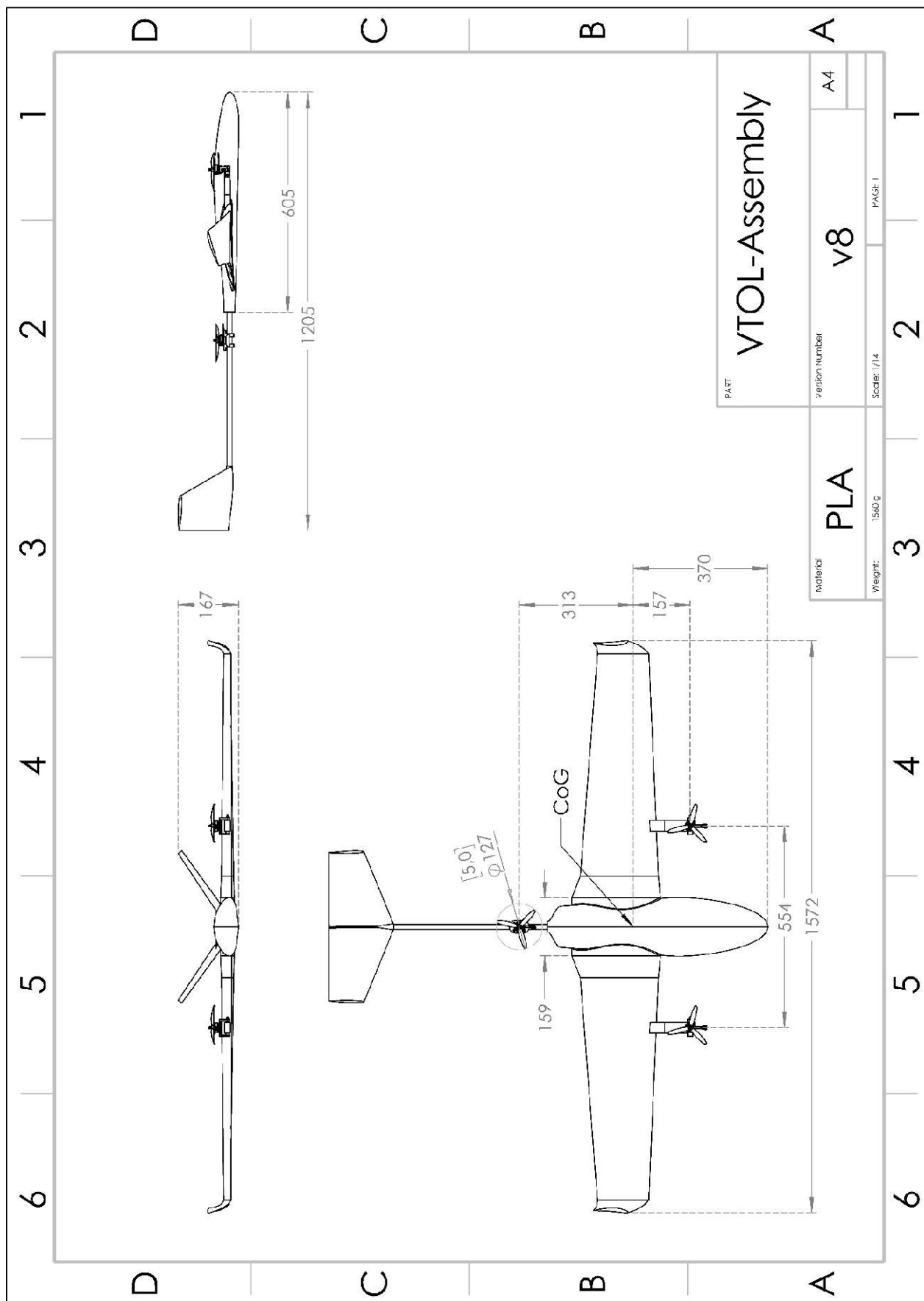
% -----Flexural Rigidity Computation-----
EI = zeros(0,length(wing_y));
for i = 1 : length(wing_y)
    if abs(wing_y(i)) < 0.084
        EI(i) = E_tube*I_tube;
    elseif abs(wing_y(i)) < L_tube
        EI(i) = E_shell*I_shell(i) + E_tube*I_tube_transformed(i);
    else
        EI(i) = E_shell .* I_shell(i);
    end
end

% -----Horizontal Flight Deflection-----
% First integration: Calculate slope
slope = cumtrapz(wing_y, M_b_hrz ./ EI);
% Adjust slope to enforce boundary condition: slope(0) = 0
slope = slope - slope(find(wing_y == 0, 1));
% Second integration: Calculate deflection
deflection = cumtrapz(wing_y, slope);
% Adjust deflection to enforce boundary condition: deflection(0) = 0
deflection_hrz = (deflection - deflection(find(wing_y == 0, 1))).*1000;

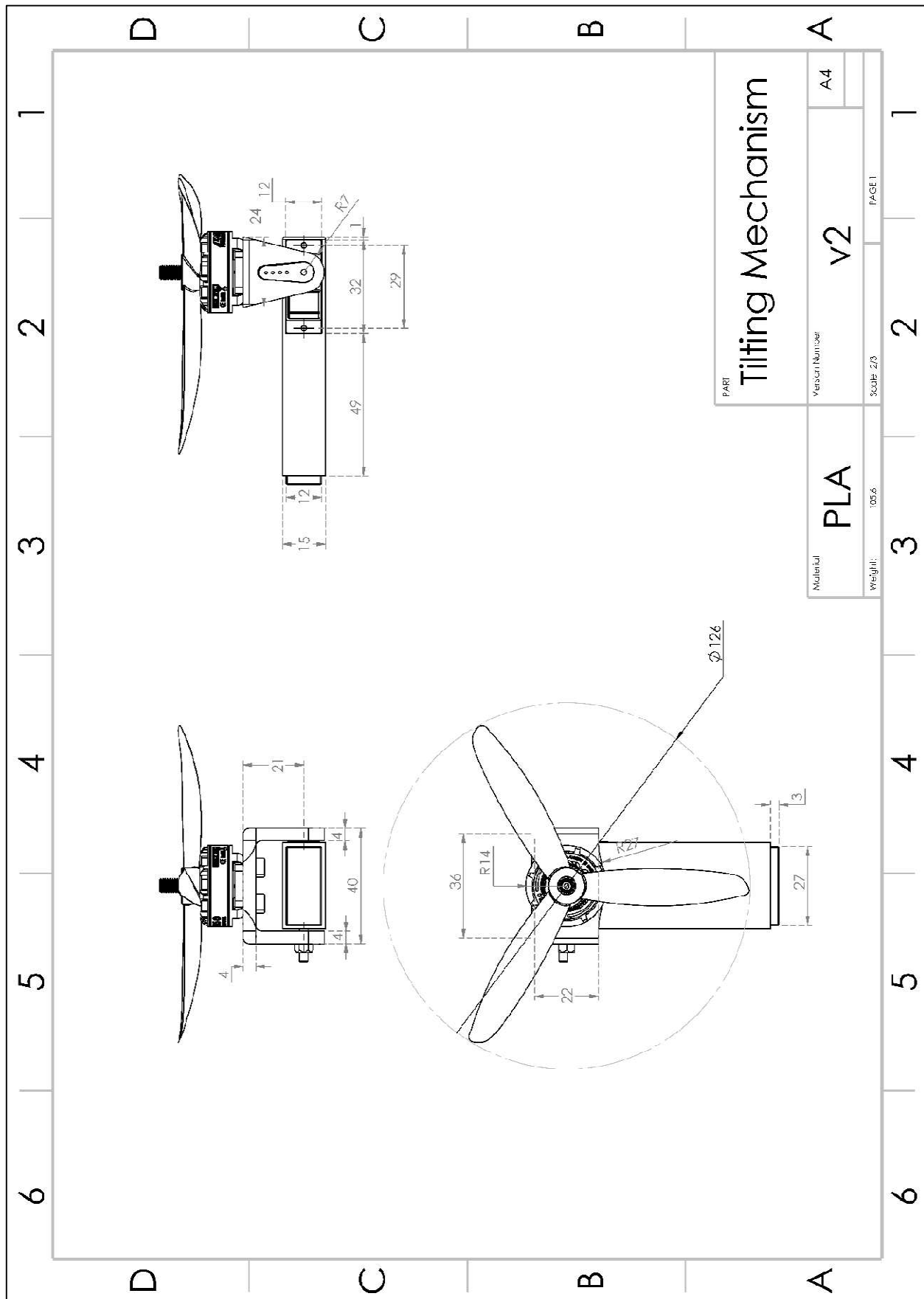
% -----Vertical Flight Deflection-----
% First integration: Calculate slope
slope = cumtrapz(wing_y, M_b_vrt ./ EI);
% Adjust slope to enforce boundary condition: slope(0) = 0
slope = slope - slope(find(wing_y == 0, 1));
% Second integration: Calculate deflection
deflection = cumtrapz(wing_y, slope);
% Adjust deflection to enforce boundary condition: deflection(0) = 0
deflection_vrt = (deflection - deflection(find(wing_y == 0, 1))).*1000;

% Plot bending moment
figure;
subplot(2, 1, 1);
plot(wing_y, M_b_hrz, 'b-', 'LineWidth', 2);
hold on;
plot(wing_y, M_b_vrt, 'r-', 'LineWidth', 2)
grid on;
xlabel('Spanwise Position [m]');
ylabel('Bending Moment [Nm]');
title('Bending Moment Distribution');
legend("during Horizontal Flight", "during Vertical Flight", Location="best");
% Plot deflection
subplot(2, 1, 2);
plot(wing_y, deflection_hrz, 'b-', 'LineWidth', 2);
hold on;
plot(wing_y, deflection_vrt, 'r-', 'LineWidth', 2);
grid on;
xlabel('Spanwise Position [m]');
ylabel('Deflection [mm]');
title('Deflection Distribution');
legend("during Horizontal Flight", "during Vertical Flight", Location="best");
```

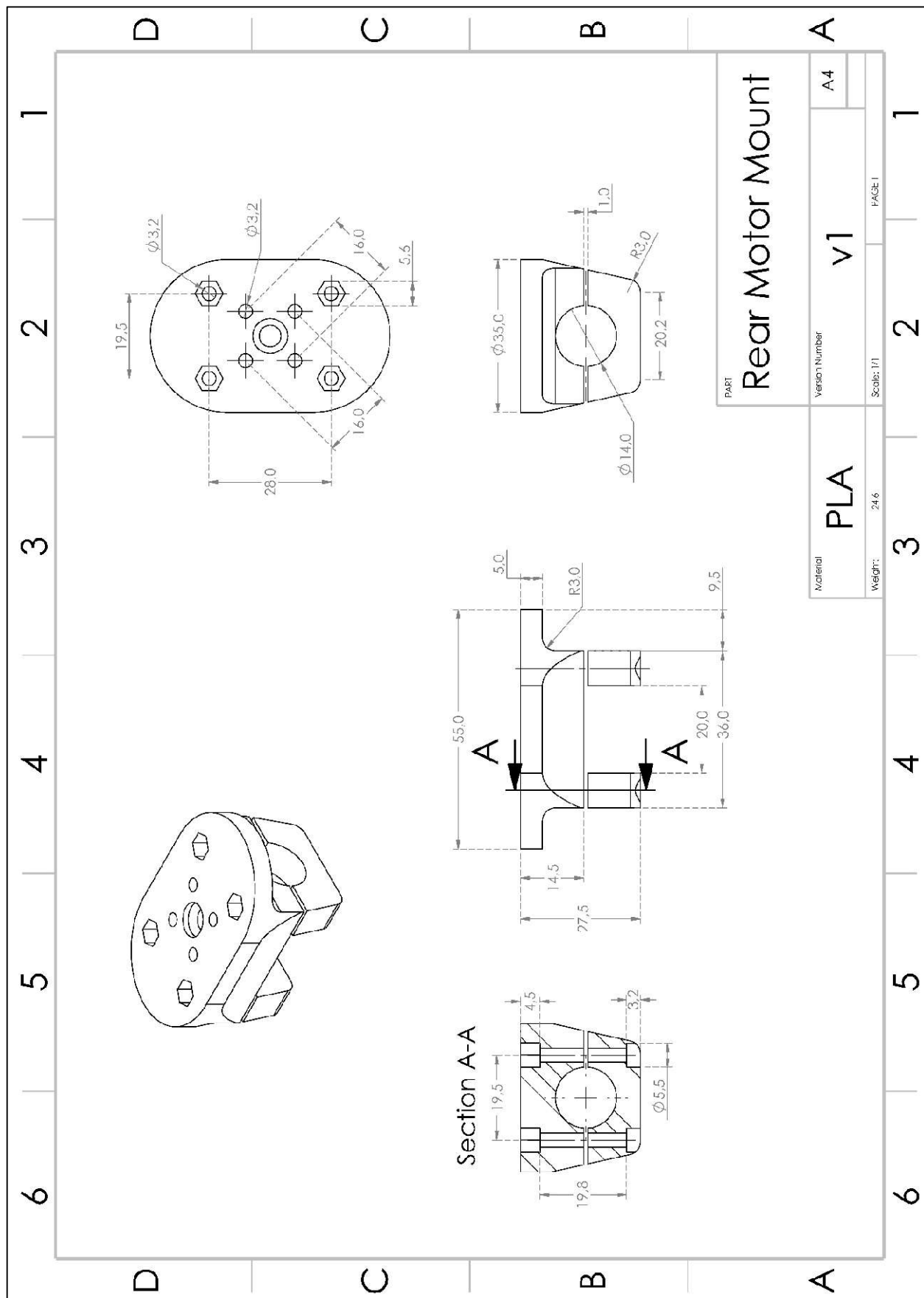
Appendix D: The Technical Drawing of the VTOL Assembly.



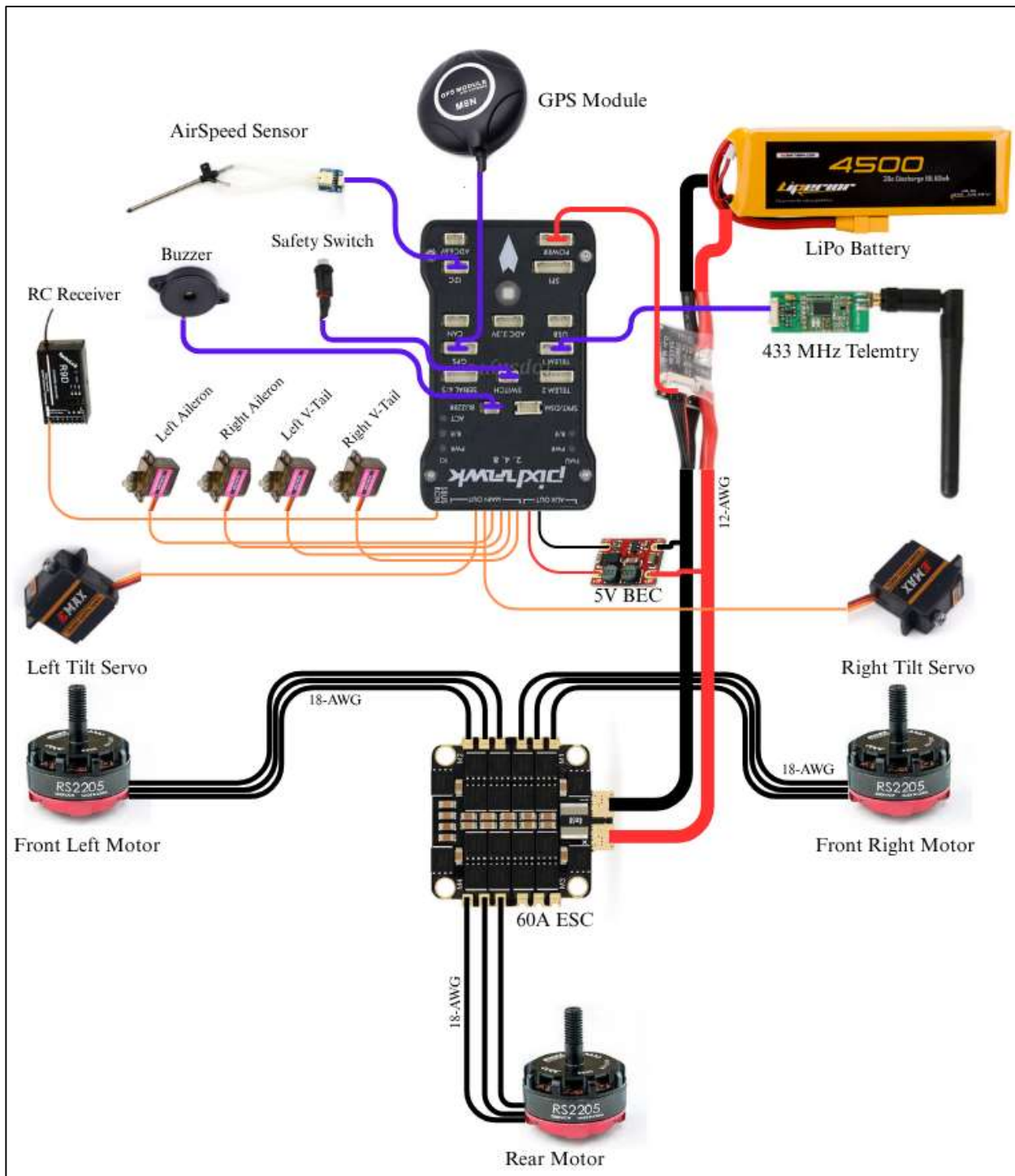
Appendix E: Technical Drawing of the Tilting Mechanism.



Appendix F: Technical Drawing of the Rear Motor Mount.



Appendix G: The Wiring Diagram of the V-TOL



Appendix H: Print Orientations of Selected Parts.

